THESIS FOR THE DEGREE OF DOCTOR OF PHILOSOPHY

Polarized light spectroscopy studies of model membranes and DNA

MAXIM KOGAN

Department of Chemical and Biological Engineering

CHALMERS UNIVERSITY OF TECHNOLOGY

Gothenburg, Sweden 2014

Polarized light spectroscopy studies of model membranes and DNA

MAXIM KOGAN

ISBN 978-91-7597-087-5

Doktorsavhandlingar vid Chalmers tekniska högskola
Ny serie nr: 3768
ISSN 0346-718X

Department of Chemical and Biological Engineering
Chalmers University of Technology
SE-412 96 Gothenburg
Sweden
Telephone + 46 (0)31-772 1000

Back cover photo by Peter Sandin

Chalmers Reproservice
Gothenburg, Sweden 2014

Polarized light spectroscopy studies of model membranes and DNA

MAXIM KOGAN

Department of Chemical and Biological Engineering
CHALMERS UNIVERSITY OF TECHNOLOGY

Abstract

Over the past decades Linear Dichroism (LD) spectroscopy has proven to be a powerful tool for studies of structure and function of different cell constituents, including DNA, cell membranes and proteins. Due to the structural complexity of cell constituents, the LD studies of biomolecules depend on development of simplified model systems, which can mimic the original structure and functionality of the cell components. The results presented in thesis concern investigation of LD model systems and include two parts. The main part of this thesis (Papers I–IV) presents investigations of cell membrane models, while the final part of this thesis (Paper V) introduces a model system that can be used for DNA studies.

Papers I and II deepen the knowledge concerning one of the most common membrane mimic - DOPC liposomes. Paper I reports on the impact of viscosity and applied shear force on the behaviour of this membrane host. Paper II demonstrated how, by using theoretical orientational models, the microscopic orientation of the sample can be monitored. Further, in Papers III–IV a new lipid model, so called bicelles, is introduced for LD studies. This lipid system can form, at certain conditions, disc-like bilayers, which we find can be aligned by shear flow, resulting in a system having low light scattering and greater orientation than liposomes.

The final part of this thesis introduces a particular kind of imperfectly paired DNA as a model system for studies of the transition-states of DNA. Probing of DNA was performed by monitoring the DNA-interaction with a bidppz-bridged binuclear ruthenium complex (ΔΔ-P) that has a known selective affinity for mismatched regions of DNA. While for native DNA, the intercalation of ΔΔ-P complex takes hours at high temperature to complete, it is demonstrated here that the ruthenium complex undergoes very rapid intercalation into re-annealed DNA already at room temperature, indicating that introduction of the static imperfectly paired DNA-structures greatly decreases the activation energy for the threading process.

Keywords: bimolecular probe, DNA, emission, linear dichroism, lipid bilayer, membrane orientation, membrane model, ruthenium dipyridophenazine complex.

List of Publications

This thesis is based on the work contained in the following papers, referred to by Roman numerals in the text:

I. Shear-Induced Membrane Fusion in Viscous Solutions
Maxim Kogan, Bobo Feng, Bengt Nordén, Sandra Rocha and Tamás Beke-Somfai
Langmuir, 2014, 30, 4875-4878

II. Probing Microscopic Interactions in Membranes
Maxim Kogan, Sandra Rocha, Tamás Beke-Somfai and Bengt Nordén
Manuscript

III. Flow-Alignment of Bicellar Lipid Mixtures: Orientations of Probe Molecules and Membrane-Associated Biomacromolecules in Lipid Membranes Studied with Polarized Light
Maxim Kogan, Tamás Beke-Somfai and Bengt Nordén
Chemical Communications, 2011, 47, 7356-7358

IV. High Anisotropy of Flow-Aligned Bicellar Membrane Systems
Maxim Kogan, Bengt Nordén and Tamás Beke-Somfai
Chemistry and Physics of Lipids, 2013, 175, 105-115

V. Transition State of Rare Event Base Pair Opening Probed by Threading into Looped DNA
Maxim Kogan, Bengt Nordén, Per Lincoln, and Pär Nordell
ChemBioChem, 2011, 12, 2001-2006

Contribution Report

Paper I — I did the major part in designing and planning the experiments; performed experimental work together with B. Feng and S. Rocha; contributed to data analysis and writing the paper.

Paper II — I did the major part in designing and planning the experiments; performed all of the experimental work; contributed to data analysis and writing the paper.

Paper III — I contributed to designing and planning the experiments; performed all of the experimental work; contributed to data analysis and writing the paper.

Paper IV — I contributed to designing and planning the experiments; performed all of the experimental work; contributed to data analysis and writing the paper.

Paper V — I performed experimental work together with P. Nordell; contributed to data analysis and writing the paper.

TABLE OF CONTENTS

1. INTRODUCTION

Over the last century, spectroscopy, i.e. the study of the interaction between matter and radiated energy, has been extensively used to increase understanding of the structure and functioning of the living cell. Development of such techniques as X-ray crystallography, nuclear magnetic resonance (NMR) spectroscopy and UV-vis spectroscopy became central for studies of living matter. The wide diversity of modern spectroscopic techniques provides a large number of tools that aid structural investigation of such cell constituents as DNA, RNA, proteins, and lipid membranes. These analytical tools continue to be developed, as new challenges and demands on sensitivity, resolution, sample concentration and purity arise.

Among the other spectroscopic techniques, linear dichroism (LD) spectroscopy has lately proved to be useful for in situ analysis of structure and function of large biomolecules, such as DNA and membrane-associated proteins.[1–3] Up to now, LD was successfully used for the structural studies of various peptides, proteins and amyloid fibrils, as well as for studies of DNA and DNA-ligand interactions.[1,4–14] Future promising investigations involve amyloid fibres and transmembrane proteins.

Working with complex cell constituents, LD depends on existence of simplified model systems, which can mimic the original structure and functionality. Instead of using real cell membrane it is often more convenient to use a simple lipid system with a known composition, particularly when studying membrane-associated molecules and proteins. These model membranes can be designed in a way that minimizes their interference with the LD signal, making the analysis of the associated molecules more direct. Also simplified models can be used when studying DNA-ligand interactions by, for example, using DNA fragments with a specific sequence or structure.

This thesis presents further development of some of the model systems used in the LD field. The first bigger part of this thesis concerns the lipid membrane systems (Papers I – IV), while the second and smaller part deals with the modelling of specific DNA structures (Paper V).

The main part of this thesis presents investigation of biological membrane models used in the LD field (Papers I – IV). Papers I and II deepen the knowledge concerning one of the most common membrane mimics – DOPC liposomes. Paper I presents the effect of viscosity and shear flow on the liposomes. It demonstrates that high viscosity liposome samples under applied shear-force show a time-dependent increase of the LD signal. This effect can be especially pronounced when shear-force is applied for long time (an hour). The resulting increase of the LD signal can be

fourfold, compared with the initial value. Paper II presents for the first time a way to characterize the microscopic alignment of the lipid bilayers in liposomes. Further, in Paper III and IV membrane model systems called bicelles are tested as a membrane host for sample orientation. The sample alignment behaviour of this membrane system shows sensitivity to such parameters as temperature, lipid concentration and lipid-mixing ratio. Moreover the experimental results indicate that using bicelles as a membrane host, under certain conditions, leads to greater sample alignment than any other flow oriented membrane system.

The final part of this thesis is based on paper V and describes how the optical spectroscopy and simplified DNA models could be used to study certain structural aspects of DNA, namely transition-state arrangement of the DNA. Generally the transition states of the DNA include unpaired regions, which are believed to be important for the binding of regulatory enzymes essential for such fundamental cellular processes as transcription, replication and recombination. In this paper, the mismatched regions of imperfectly paired model DNA were tested by DNA-ligand interactions using the binuclear ruthenium complex (ΔΔ-P) that has a known selective affinity for mismatched regions. The results show that imperfectly paired DNA can be used as a model for the transient DNA conformation.

This Thesis has the following structure: basic concepts important for the present research are summarized in Chapter 2; the following Chapter 3 describes relevant theory and methods which provide the foundation for the present research; further, Chapter 4 provides a short summary of the results presented in Papers I – V followed by concluding remarks given in Chapter 5.

2. BASIC CONCEPTS

2.1 Studying the cell

The cell is the smallest structural, functional and biological unit of life in the living organism. For unicellular organisms (e.g. bacteria and protozoans) a single cell accomplishes all life functions, while in multicellular organisms (e.g. animals and plants) differentiation of cells into specialized tissues takes place. Nevertheless all cells share common properties: storage of gene information encoded in DNA; synthesis of proteins in the cell's ribosomes using the mRNA transcript of DNA; usage of proteins as structural material, as enzymes and for cell signalling; usage of adenosine triphosphate as a storage of energy; and encapsulation of the cell by a membrane, composed of lipid molecules and embedded proteins.

The studies of cells, called cell biology, has a long history beginning from 1665 with the publication of Robert Hooke's *Micrographia*.[15] Due to the microscopic dimensions, gaining knowledge of cell structure depended on development of analytic instruments and associated experimental techniques. Modern methods used for cell studies include spectroscopic techniques, x-ray crystallography, microscopic techniques, nuclear magnetic resonance (NMR) etc. Due to the complexity of cells, many experimental techniques require the use of simplified models of the cells or of its constituents. The following sections provide details regarding biological molecules and biological models used in this thesis.

2.2 Modelling cell membranes

The cell membrane is a complex structure that separates the interior of the cell from the outside environment. Apart from being a permeable barrier it plays several critical roles in cell function. The cell membrane anchors the cytoskeleton providing and maintaining cell shape. The membrane hosts proteins involved in the transport of molecules into and out of the cell. Also the membrane plays an important role in energy conservation in the cell.[16] The core structure of a mammalian cell membrane consists of a phospholipid bilayer built from four common phospholipids: phosphatidylcholine (PC), phosphatidylethanolamine (PE), phosphatidylserine (PS), and sphingomyelin (SM). Apart from the lipids, the membranes of animal cells contain sterols, glycolipids and proteins, which may constitute up to 50% by weight of membrane content.[17]

Membrane proteins (20–30% of the total proteome)[18] have a broad structural and functional diversity facilitating many important processes in living cells. They are involved in cell-cell signalling and intracellular interactions. Also they play an important structural roll anchoring cytoskeletal proteins to the cell membrane. Moreover trans-membrane proteins aid and regulate transport of molecules across the membrane.[19]

Membrane proteins generally have several transmembrane segments with different orientations in the membrane. The hydrophobic regions of the segments are usually embedded in the cell membrane, while hydrophilic regions are located outside of the phospholipid bilayer. Therefore removal of the protein from the cell membrane into polar or non-polar solvents usually changes its 3D structure. This structural change in combination with low concentration levels in the cell creates difficulties for structural studies of membrane proteins. At present, the atomic 3D structures are determined for less than 0.1% of all membrane proteins.[20]

Structural studies of membrane proteins often require insertion of the purified protein into the reconstituted membrane. For instance supported bilayers, micelles and large unilamellar vesicles (LUVs) are some of the lipid systems used in linear dichroism spectroscopy, the main technique applied in this thesis.[21] The main building blocks of biomembranes are phospholipids, which are a class of amphiphilic molecules that contain two hydrophobic tails and a phosphate-containing hydrophilic head group (Figure 2.2.1). Phospholipids have the ability to spontaneously aggregate in aqueous solutions. Micelles, lipid bilayers and liposomes are some of the aggregates that can be formed by lipids, depending on the length and saturation of their tails likewise the nature of their headgroups (Figure 2.2.1). Liposomes with a diameter of 100 nm are the most commonly used membrane system for LD studies.

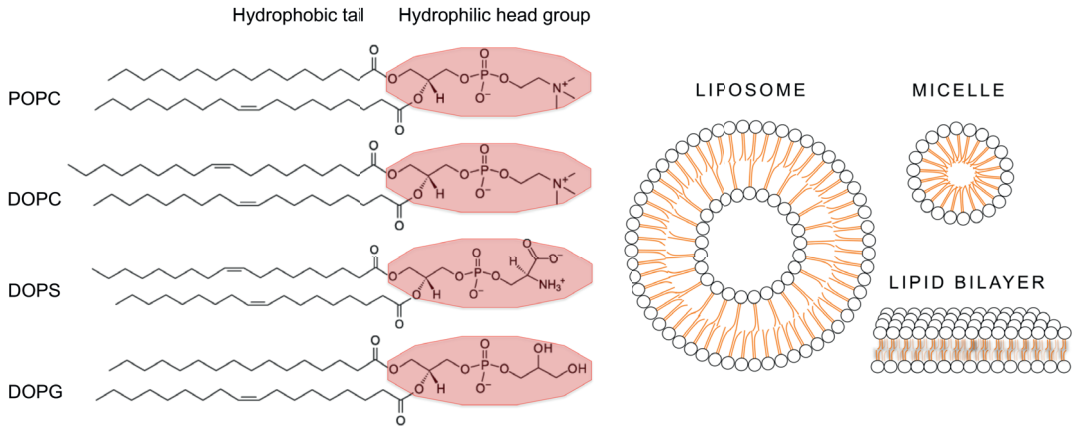

Figure 2.2.1. Left: Schematic structures of common phospholipids used for liposomal preparation; **Right:** Some of the aggregates formed by phospholipids in aqueous solutions.

Liposomes As A Model System For Linear Dichroism

Deformation of the spherical form of the liposome into an ellipsoid can increase the alignment of its comprising lipid bilayers (Figure 2.2.2). Linear dichroism works with aligned samples and flow orientation by a shear force created in Couette flow cells is the most common method used for liposome alignment. Still some of the drawbacks of this model membrane are the low orientation even at high shear forces (3100 s^{-1}) and high light scattering demanding short path-length and high sample concentrations. However over time it has been shown that the orientation of liposomes can be improved by cholesterol addition that increases the membrane rigidity,[22] or by adding sucrose, which rises the medium viscosity and minimizes light scattering.[4]

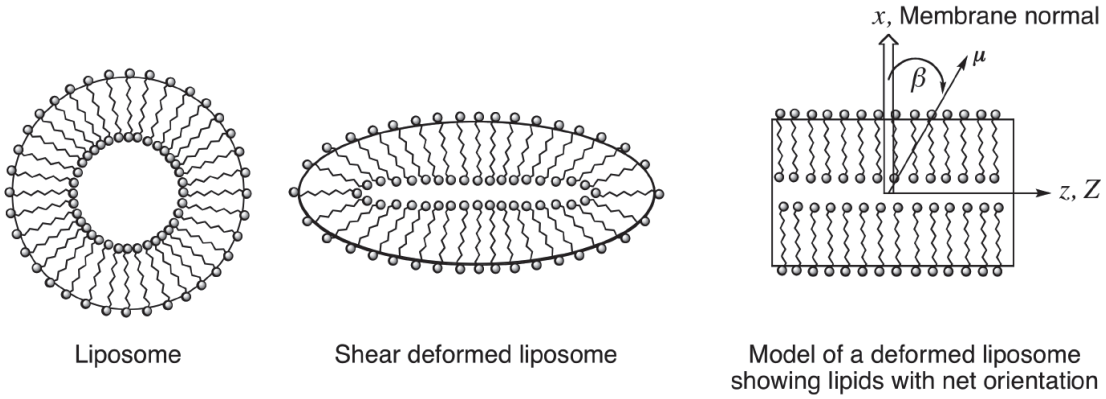

Figure 2.2.2. Left: a schematic representation of a liposome**; Centre:** shear deformed liposome**; Right:** a lipid bilayer with lipids having a net orientation. Reproduced by permission of The Royal Society of Chemistry.[21]

Bicelles

Bicelles are a class of model membranes that are usually prepared with two lipids, one of which forms a flat lipid bilayer while the other forms an amphipathic, micelle-like assembly protecting the bilayer from the surrounding solvent.[23] The composition and morphology of bicelles mimic well common PC-rich eukaryotic membranes, therefore they are extensively used for structural studies of membrane-associated peptides, especially in the NMR field.[24,25] The most commonly used bicelles are prepared from the following phospholipids mixed at different molar ratios: 1,2-dihexanoyl-sn-glycero-3-phosphocholine (DHPC) and 1,2-dimyristoyl-sn-glycero-3-phosphocholine (DMPC) (Figure 2.2.3). Generally, the bicellar mixtures are characterized by two parameters: the lipid molar ratio, $q=[DMPC]/[DHPC]$ and total weight percent of the lipids in a buffer, c.

The most common composition of DMPC/DHPC used in NMR studies has the lipid content between 20–30% and q=3.2.[25] The morphology and phase behaviour of such mixtures are quite complex (Figure 2.2.3) and it strongly depends on the temperature and molar mixing ratio. The bicelle formation typically occurs in a certain temperature region that has to be experimentally determined for each lipid composition.

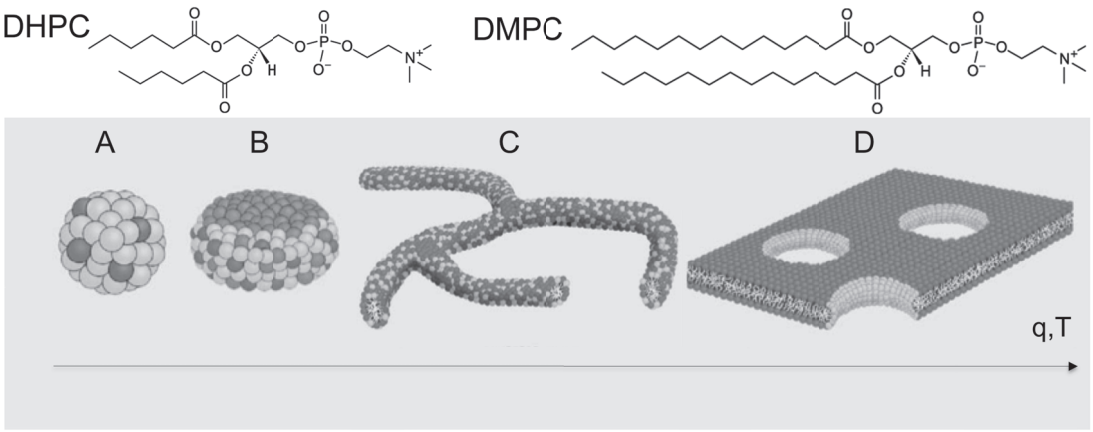

Figure 2.2.3. The structure of common morphologies of DMPC/DHPC bicelles as a function of temperature (T): **A)** mixed globular micelle, **B)** bicelle; **C)** wormlike micelle; **D)** holey lamellar sheet. Black head groups represent DMPC and light-grey head groups represent DHPC. Reprinted from reference[26] with permission from Elsevier.

In this thesis (Papers III-IV) we introduce bicelles as a promising new membrane model for linear dichroism spectroscopy. Our results showed high flow alignment of lipid bilayer in bicellar mixtures. Moreover we performed detailed characterization of lipid alignment over a broad range of conditions including lipid concentration, temperature, lipid mixing ratio and shear gradient. Finally we demonstrate that flow oriented bicelles can be used for biophysical studies of membrane-associated systems.

2.3 DNA

Deoxyribonucleic acid (DNA) is a long polymer chain that contains the complete genetic information needed for the development and functioning of every living organism. According to the central dogma of biology, the genetic code of DNA is transcribed to RNA and subsequently translated into the proteins that perform most of the work required for maintenance and function of the cell.[27] The structure of DNA was resolved by Watson and Crick in 1953,[28] who found it to be a double helix consisting of two long polynucleotide chains, so called strands, composed of four types of nucleotide sub-units: adenine (A), cytosine (C), guanine (G), and thymine (T) (Figure 2.3.1). While thymine base-pairs with adenine by creating two hydrogen bonds, the cytosine forms three hydrogen bonds with guanine. The G–C interaction is therefore significantly stronger (by about 30%) than A-T, causing the A–T rich regions to be more inclined to thermal fluctuations.

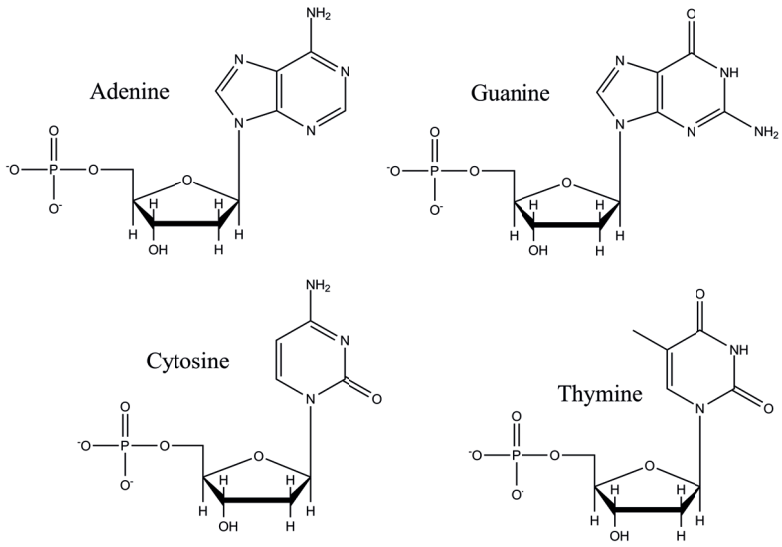

Figure 2.3.1 The four DNA nucleotides: adenine (A), cytosine (C), guanine (G), and thymine (T).

The most abundant form of DNA in the cell is B-DNA that has the shape of a right-handed helix with anti-parallel strands and a twist of 36° per each base-pair. The DNA bases are located perpendicular to the long axis of DNA, approximately 3.4 Å apart, creating a local hydrophobic environment. Each of the phosphate groups carries a negative charge making DNA a polyanion at physiological pH. The overall structure of DNA is asymmetric, having a narrow minor groove and a broader major groove.

The structure of the double helix allows a broad variety of interactions with other molecules - from large proteins to small synthetic molecules. These interactions include such binding modes as intercalation, groove-binding and electrostatic interaction (Figure 2.3.2). For instance, the dumb-bell shaped binuclear ruthenium

complex employed in this Thesis (Paper V) has two binding modes. Initially, it binds outside or in either groove of the double helix and subsequently threads one of its bulky subunits through the core of the DNA placing a dppz-bridging moiety between the bases. This final binding mode is called "threading intercalation" and it is a very slow process that requires several hours to completion when using mixed-sequence DNA.

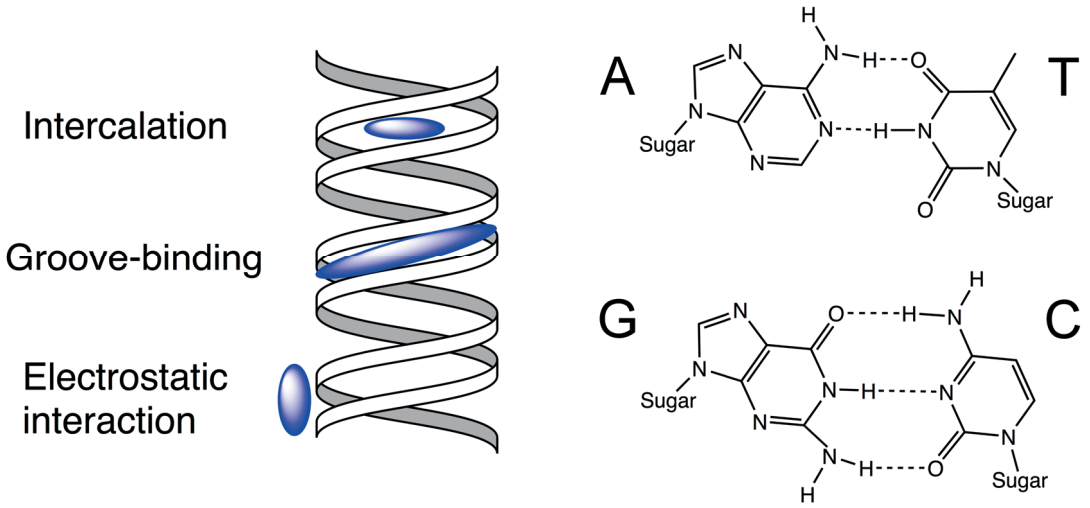

Figure 2.3.2. Left: The model of the B-DNA double helix and schematic representation of possible interactions between ligands and DNA; **Right:** hydrogen bonds between complementary DNA bases.

A single DNA strand is kept together by the covalent bonds between sugars and phosphates of the nucleotides. When two single strands form a double helix it is held together by hydrogen bonds between the base pairs (Figure 2.3.2). Hydrogen bonds are relatively weak and can be broken and re-joined relatively easily; therefore, local disruptions between DNA strands occur frequently.[29] Under those structural fluctuations, the specific binding sites on the single strands of DNA are getting exposed and therefore accessible for the various regulatory protein complexes. Therefore this process, known as DNA breathing, is essentially important for such fundamental cellular processes as replication, transcription and recombination of DNA.[17,30]

When studying the transient DNA conformation, different DNA constructs were previously used to model structural fluctuations including AT-DNA, thermal-denatured DNA, DNA replication fork constructs, DNA hairpins and other well-defined sequences of short oligonucleotides.[31–34]

2.4 LD and chemical probes for monitoring properties of lipid membranes and DNA

Linear dichroism is the main spectroscopic technique used in this thesis. This method requires usage of chemical probes for orientation, visualization and quantitation when working with biological samples. There is a broad variety of known LD probes with different structural and physical properties. Generally probes can be divided into two main groups - intrinsic and extrinsic. Intrinsic probes occur naturally and include for example aromatic amino acids and DNA bases. By contrast, extrinsic probes are added to the sample. Thus small aromatic molecules (e.g. retinoids, pyrene) are useful extrinsic probes for determining the lipid bilayer orientation, when working with lipid membranes. Contrary, determination of DNA orientation is usually done using the intrinsic absorption of DNA bases at 260 nm (assuming the angle of the transition moments being 86°).[21] Furthermore there is a broad variety of DNA ligands frequently used as LD probes with a known angle of binding, including ethidium bromide, netropsin, 4,6-diamidino-2-phenylindole (DAPI), Hoechst 33258 and different metal complexes.[21,35] Here follows a brief description of the probe molecules used in this Thesis.

Retinoic Acid

An accurate determination of angles between the membrane normal and transition dipole moments of membrane-associated molecules is one of the advantages of the LD technique. However probes with a known angle of insertion are needed in order to estimate the orientation of the lipid bilayers. Previous research indicated that some retinoids could be useful for this purpose.[22,36] This group of vitamin A derivatives consists of hydrophobic rod-like molecules (Figure 2.3.3) that have the ability to insert efficiently into the membrane bilayer parallel to the lipid chains.

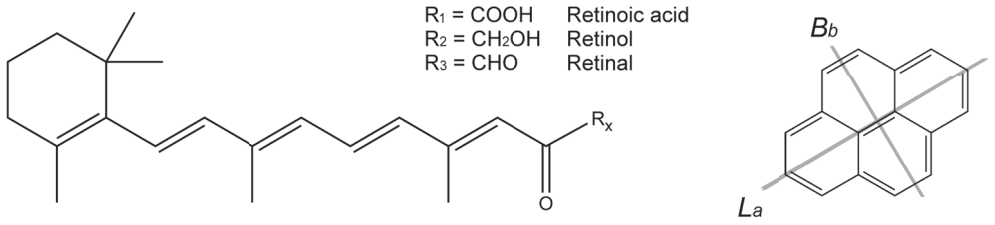

Figure 2.3.3 Left: Molecular structure of retinoids in their all-trans configuration. **Right:** Molecular structure of pyrene; *La* and *Bb* are indicating two orthogonal transition moments of the molecule.

Among the other retinoids, retinoic acid (RetA) demonstrates significantly better orientation in lipid membranes, which makes it a probe-of-choice for the estimation of the orientation factor parameter, S.[22] The transition moment of this probe is oriented along the long axis of the molecule and it has one single absorption band in the visible region of the spectra with a peak at around 350 nm. The insertion angle between the dipole moment and the membrane normal is assumed to be zero. In this thesis RetA was used as a main probe for determination of macroscopic orientation of the shear-deformed liposomes and bicelles in Papers I–IV.

Pyrene

Pyrene is a flat aromatic molecule that has orthogonal transition dipole moments polarized in the plane of the molecule (Figure 2.3.3). The L_a transition (340 nm) is polarized parallel to the long axis of the molecule, while B_b (275 nm) transition is perpendicular to the long axis. Due to the hydrophobic nature of this molecule it inserts into the lipid membranes with the long axis preferably parallel to the lipid chains. Mixed with DNA, pyrene inserts between neighbouring base pairs of a double helix.[37,38] When working with lipid bilayers, the ratio between the two orthogonal transition moments can be used to discriminate between rod-like or disk-like behaviour of the probe in the bilayer. Therefore, this probe can provide additional information about the lipid system, contrasting RetA that only has one transition dipole moment accessible in the visible region of the electromagnetic spectrum.

Curcumin

Curcumin is a major polyphenolic pigment of the root turmeric that is widely cultivated in tropical parts of Asia.[39] Turmeric is commonly used as a spice (curry) and also as a traditional medicine in India and China. Recent research indicates that curcumin exhibits potential therapeutic properties and may be used against inflammatory, cardio-vascular and skin diseases. At the moment there are several phase I and II on-going clinical trials on curcumin for the treatment of Alzheimer's disease and also for the treatment of different forms of cancer.[40] Curcumin is also used as a solvent-sensitive fluorescent probe that interacts with proteins and the cell membrane.[40,41]

Curcumin can exist in several tautomeric forms, including a 1,3-diketo form and two equivalent enol forms. In solutions at physiological pH it is normally present in keto-enol tautomer form (Figure 2.3.4).[42] When added to lipid samples at physiological pH, curcumin binds to the surface of bilayers - in contrast with RetA and pyrene, which insert into the membrane. In this Thesis curcumin was used in Paper II as a probe for lipid membrane alignment of liposomes. Our previous

(unpublished) results indicate that curcumin has far better orientation at the lipid bilayer than retinoic acid. Also it has a non-overlapping spectrum with pyrene (also used in Paper II) so it was possible to measure LD and absorption with both probes added to the sample.

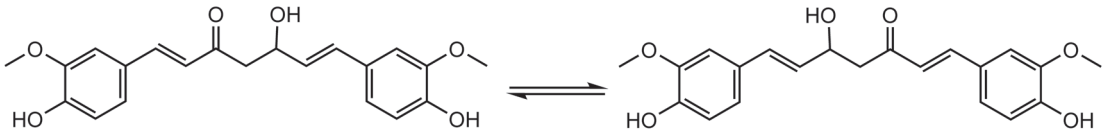

Figure 2.3.4 Solution structures of curcumin: two asymmetric keto-enol tautomers.

Binuclear Ruthenium complex

Research concerning interactions between DNA and ruthenium polypyridyl complexes started more than 30 years ago, when Barton and co-workers investigated DNA binding of $[Ru(L)_3]^{2+}$ (L = bipyridine (bpy) or phenanthroline (phen)).[43,44] During the following years ruthenium complexes were proved to be strong DNA binders with useful photo-physical properties. Non-covalent types of interactions (e.g. intercalation, electrostatic or surface binding), between DNA and ruthenium complexes result in a reversible kind of binding, keeping both molecules intact. Additionally the octahedral coordination geometry around the ruthenium ion permits variation of the ligands, which allows modification, and fine-tuning of physical and chemical properties. One such modified binuclear ruthenium complexes was used as a probe in this Thesis (Paper V). The structure of $[\mu\text{-(bidppz)(phen)}_4Ru_2]^{4+}$ (ΔΔ-P) is shown in Figure 2.3.5.

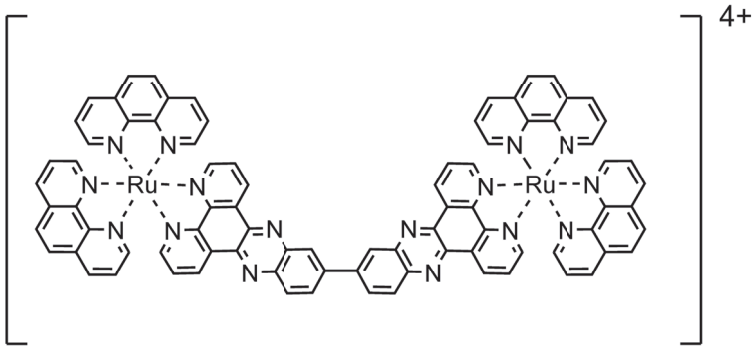

Figure 2.3.5 Chemical structure of $[\mu\text{-(bidppz)(phen)}_4Ru_2]^{4+}$, where bidppz = 11,11'-bis (dipyrido [3,2-*a*:2',3'-*c*] phenazinyl) and phen = 1,10-phenanthroline. The coordination of the ruthenium centre allows two stereoisomeric forms. The homochiral right-handed complex ΔΔ-P has been used in this Thesis.

This type of ruthenium complex displays slower DNA association and dissociation rates, making them promising therapeutic agents.[45,46] Furthermore this type of molecules may act as "light switches" when mixed with DNA, i.e. they emit no luminescence in aqueous buffers, but when intercalated to DNA, they show intense luminosity.[45,47,48]

Linear dichroism spectroscopy is a technique that may be used to sensitively display the kinetics of the DNA–ΔΔ-P interactions and reveal binding geometry changes. The first groove-binding mode, adopted upon mixing, shows positive linear dichroism of the bidppz-ligand at 320 nm.[49] With time, the ruthenium complexes undergo intercalation into DNA – a generally extremely slow process that may take hours even at elevated temperature and which can be characterized by a change of LD at 320 nm from positive (groove binding) to negative (intercalation).[13,50] This LD shift together with the "light-switch" effect was used while investigating various DNA constructs presented in Paper V of this Thesis.

3. THEORY AND METHODOLOGY

In this section an overview of the techniques used in this Thesis is presented together with a short theoretical background. More details about the experiments performed in this Thesis can be found in the appended articles.

Spectroscopy is the study of interaction between matter and electromagnetic radiation. The principle of this technique is based on the fact that different atoms and molecules interact with light in a specific way, which is giving rise to a unique interaction spectrum. The uniqueness of this spectrum makes it sometimes possible to detect and assign small changes in molecular structure and a molecular environment, which makes spectroscopic methods very useful in physical and analytical chemistry. There is a broad variety of spectroscopic techniques, which address different types of light-matter interactions such as absorption, emission, scattering and many others. Below is a brief review of the spectroscopic techniques used in this thesis. A more detailed description of spectroscopy in general and of fluorescence spectroscopy, polarized spectroscopy and light scattering in particular, can be found in the textbooks by Hollas,[51] Lakowicz,[52] Nordén *et al.*[21] and Berne *et al*.[53]

3.1 Absorption

Absorption of electromagnetic radiation is the process by which the energy of a photon is taken up by matter, typically the electrons of an atom or a molecule. During this process molecules or atoms undergo an excitation to a higher energy level. The probability of light absorption (A) by an individual molecule in a sample is related to the angle (α) between the electric field of the incident electromagnetic radiation and the electric dipole transition moment of the molecule (μ),

$$A \propto |\mu|^2 cos^2\alpha \qquad (3.1.1)$$

In order for absorption to take place the energy of the photon must match the energy gap between the electronic states of the molecule (Figure 3.1.1), as formulated by the Bohr frequency condition:

$$\Delta E = E_{higher} - E_{lower} = h\upsilon \qquad (3.1.2)$$

where h is the Planck's constant and ν is the frequency of absorbed light.

Absorbance is defined as a logarithm of the ratio between the incident (I_o) and transmitted light (I) intensities and is related to the concentration (c), path length (l) and the extinction coefficient (ε) of the molecule according to the Beer-Lambert law:

$$A = log\frac{I_0}{I} = \varepsilon cl \qquad 3.1.3$$

In the expression above, the logarithm is used in order to get a linear relation between absorbance and concentration, mainly for simplicity of calculations.

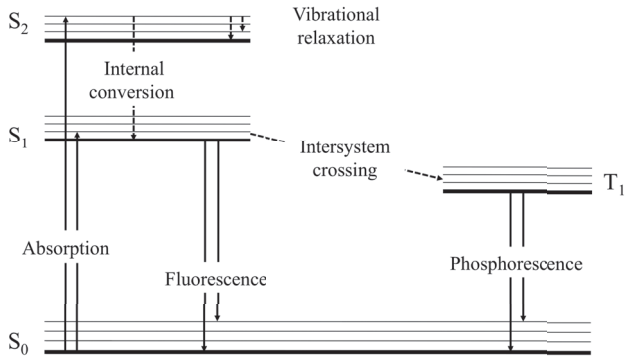

Figure 3.1.1 A Jablonski diagram showing excitation levels and possible excitation and relaxation pathways.

Absorption spectroscopy was used in this thesis mainly during the preparation of stock solutions and samples to determine their concentrations. In Papers I–IV absorption measurements were also used for LD^r calculations. Finally in Paper V the absorption spectroscopy was used for the analysis of heat-denatured DNA and for obtaining the melting curves of the investigated DNA constructs.

3.2 Fluorescence

Following the absorption of a photon, the molecule undergoes, in most cases, a rapid relaxation back to the lower energy state. This occurs due to the instability of the excited states of the molecule. Different pathways of relaxation are often summarized in a Jablonski diagram. In Figure 3.1.1 the following electronic states are represented: the first and second excited states, S_1 and S_2; the energy ground state S_0 and the first triplet excited state, T_1. Transitions between the energy levels represented in the Jablonski diagram can be divided into radiative, that is the emission of photons, or non-radiative, when the energy is transferred to the surrounding in a non-emissive way; such as kinetic energy. The ratio between radiative and non-radiative relaxation is defined as the efficiency of fluorescence or quantum yield:

$$\Phi = \frac{number\ of\ photons\ emitted}{number\ of\ photons\ absorbed} \qquad (3.2.1)$$

Figure 3.1.1 shows two radiative pathways: *fluorescence*, a transition from the energy level S_1 to S_0 and *phosphorescence*, a transition from T_1 to S_0. Due to the different electron spin configuration of the S_1 and T_1 levels they have different rates of photon emission. While phosphorescence is a slow emittive process that can take several hours, fluorescence occurs very rapidly on the timescale of 10^{-9} to 10^{-7} seconds.

Fluorescence spectroscopy allows the analysis of fluorescence arising from a sample containing molecules of a certain compound. The instrumental set-up involves a light source, commonly emitting light in the UV region, that excites the electrons in molecules. The subsequent emission of the light by the electrons, typically in the visible spectrum, is recorded by the detector usually placed at the right angle to the excitation light.

In this thesis, fluorescence spectroscopy was used in Paper I to monitor liposome fusion (explained in more details in the next subchapter "Förster Resonance Energy Transfer"). In Paper V, fluorescence measurements were used to study the interactions between ruthenium complex and different types of DNA molecules.

Förster Resonance Energy Transfer

One of useful tools in fluorescence spectroscopy is Förster resonance energy transfer (FRET). The general principle of this technique is the energy transfer from a donor molecule (D) to an acceptor molecule (A) through dipole-dipole interactions. The transfer of energy may occur if emission spectrum of a donor has a spectral overlap with the absorption spectrum of the acceptor. The efficiency of FRET

depends, among other conditions, on the quantum yield of D, the relative orientation of the dipole moments of D and A and on the distance between D and A. The latter makes it possible to use FRET as a spectroscopic ruler for the estimation of the distance between molecules. Hence energy-transfer efficiency, *E*, is related to the distance between the donor and acceptor by:

$$E = \frac{R_0^6}{(R_0^6 + r^6)} \qquad (3.2.2)$$

where r is the distance between the donor and the acceptor and R_0 is the Förster distance (i.e. the distance at which the energy transfer efficiency between D and A is 50%). Typically, R_0 varies between 20 and 60 Å, making it possible to estimate distances up to 90 Å between standard FRET-pairs with reasonable accuracy.

In this thesis lipid-mixing FRET assay was used in Paper I to monitor vesicle fusion, using a FRET pair including N-(7-nitrobenz-2-oxa-1,3-diazol-4-yl) phosphoethanolamine (NBD-PE) and N-(lissamine rhodamine B sulfonyl) phosphoethanolamine (Rh-PE). In short, low concentrations of both NBD-PE and Rh-PE were added to one batch of lipid vesicles, allowing an efficient energy transfer between the donor (NBD-PE) and the acceptor (Rh-PE). This batch of labeled liposomes was mixed with unlabeled liposomes at a molar ratio of 1:9. When membrane fusion occurs between labeled and unlabeled liposomes the average distance separating the FRET pair increases, leading to a decrease in the efficiency of the energy transfer. The latter can be monitored by fluorescence spectroscopy. A more detailed FRET assay description can be found in the publication by Duzgunes et al. 2010.[54]

3.3 Linear Dichroism

Linear dichroism (LD) is a spectroscopic technique measuring differential absorption of linearly polarized light (i.e. light that consists of photons with electric field vectors oscillating in a given plane along the propagation direction). By definition

$$LD = A_{II} - A_{\perp} \tag{3.3.1}$$

where A_i denotes absorption of light polarized parallel (A_{II}) and perpendicular ($A_{\perp}$), respectively, to some macroscopic orientation direction. Isotropic samples do not show LD due to random orientation of molecules, so in order to measure LD the sample must be aligned. In that case the absorption intensity will be proportional to the squared cosine of the angle θ between the electric field vector of incident light and the electric dipole transition moment μ of the molecule:

$$A \propto |\mu|^2 \cos^2\theta \tag{3.3.2}$$

If the transition moment is oriented parallel to the orientation axis, then $A_{II} > A_{\perp}$ and the resulting LD will be positive. Conversely, if it is oriented perpendicular to the orientation axis, then $A_{II} < A_{\perp}$ giving a negative value of LD.

The LD signal depends on the sample concentration and the sample path-length, which follows from the Beer-Lambert law (Eq. 3.1.3). Often it is more convenient to normalize LD with respect to the isotropic absorption of the sample, resulting in a reduced LD, or LD^r:

$$LD^r = \frac{A_{II} - A_{\perp}}{A_{iso}} \tag{3.3.3}$$

LD^r is thus independent of sample concentration and sample path length.

Flow linear dichroism

As mentioned above, LD technique requires an oriented sample. Several methods of sample orientation are available for LD measurements including electric or magnetic orientation, stretched polymers, gels etc. In this thesis a shear-flow orientation was used to create sample alignment. Figure 3.3.1 shows the main principle of the flow LD using the outer-rotating Couette flow-cell. The sample is placed in the narrow gap between a transparent outer quartz cylinder and a stationary transparent inner quartz cylinder. Rotation of the outer cylinder creates a laminar shear flow that can be used for sample alignment. While such long and stiff polymers as DNA can be easily oriented along the flow direction, small molecules remain statistically randomly oriented in solution. In order to flow-align small molecules they can be solubilized in

some sort of matrix having an orientation axis. This matrix can be a stretched plastic film, a lamellar liquid crystal, a DNA double helix, or a flow-deformed liposome. The last mentioned form of membrane system was used for research presented in this Thesis.

The efficiency of macroscopic orientation of the molecules in the sample can be described by a parameter termed orientation factor S: for perfectly aligned samples S = 1 and for isotropic samples S = 0. The S value for such systems as liposomes or DNA can be determined from LD using a molecule with a known angle of insertion.

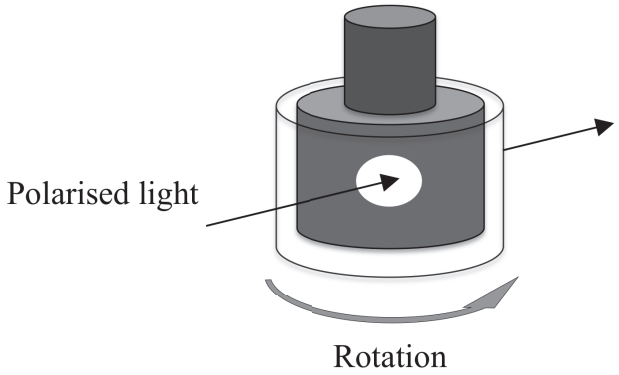

Figure 3.3.1 A schematic representation of the outer rotating cylinder Couette flow cell

Uniaxial samples

Uniaxial orientation demands an oriented system in which the transition moment lies at a certain angle relative to a local reference axis in such a way that all orientations on a cone around this reference axis are equally probable (Figure 3.3.2). In many LD experiments the uniaxial orientation of the sample can be assumed when investigating molecules solubilized in most stretched films and liquid crystals, but also for helical structures such as DNA.[55] The orientation fields created in Couette flow cells generally have lower macroscopic symmetry than uniaxial. In this case a uniaxial orientation can still be assumed locally (cylindrical DNA or cylindrically deformed liposomes), but S parameters for the macroscopic orientation have to be experimentally determined from LD of an absorption band with known angle of insertion θ_z.[21] Figure 3.3.2 (left) presents the macroscopic coordinate system XYZ, where Z is the orientation direction. Using this laboratory frame, the orientation angles can be defined for any arbitrary transition moment μ. In the case of a uniaxially oriented sample (Figure 3.3.2) the arbitrary transition moment μ adopts a define angle θ_z to the Z-axis, while all values of the azimuthal angle Φ are equally probable. Consequently, absorption spectra measured perpendicularly to the orientation axis will be identical, resulting in only two independent absorption parameters:

$$A_Z = A_{II} = \kappa|\mu|^2 \cos^2\theta_Z$$
$$A_X = A_Y = A_\perp = \kappa|\mu|^2 \sin^2\theta_Z \sin^2\Phi \quad (3.3.4)$$

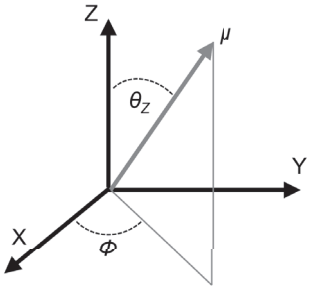

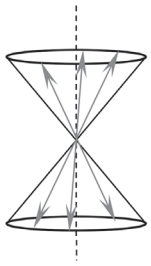

Figure 3.3.2 Left: Coordinate system defining the laboratory frame (XYZ). The orientation of a transition dipole moment μ is described by the angles Φ and θ_Z. **Right:** Uniaxial orientation around the Z-axis. All orientations of the transition moment, which are confined to the geometry of the cone, are equally probable.

Thus

$$LD = A_z - A_Y = \kappa\mu^2 (\cos^2\theta_Z - \sin^2\theta_Z \sin^2\Phi) \quad (3.3.5)$$

Similarly, the isotropic absorbance, A_{iso} can be described as:

$$A_{iso} = \frac{A_Z + A_Y + A_X}{3} = \frac{A_Z + 2A_Y}{3} = \frac{1}{3}\kappa\mu^2(\cos^2\theta_Z + 2\sin^2\theta_Z \sin^2\Phi) \quad (3.3.6)$$

Since the values of Φ are not restricted, the values of $\sin^2\Phi$ can be averaged between 0 and 2π giving $\langle \sin^2\Phi \rangle = {}^1/_2$. Therefore

$$LD = \frac{\kappa\mu^2}{2}(3\cos^2\theta_Z - 1) \quad (3.3.7)$$

$$A_{iso} = \frac{\kappa\mu^2}{3} \quad (3.3.8)$$

Combining equations 3.3.7 and 3.3.8 and correcting for the non-perfect sample orientation by using the orientation factor S results in:

$$LD^r = \frac{3}{2}S(3\cos^2\theta_Z - 1) \quad (3.3.9)$$

This expression sets upper and lower limits of the LD^r values to $3S$ and $-\frac{1}{2}S$. The above expression can be used for molecules flow-oriented in DNA matrix.

Shear-deformed liposomes

Liposomes deformed by a shear flow can be treated as cylindrical systems (Figure 3.3.3) where the solubilized analytes have a uniform orientation about the orientation axis of the cylinder. In this case equation 3.3.9 cannot be used to describe the LD but an additional element of rotational averaging is required.

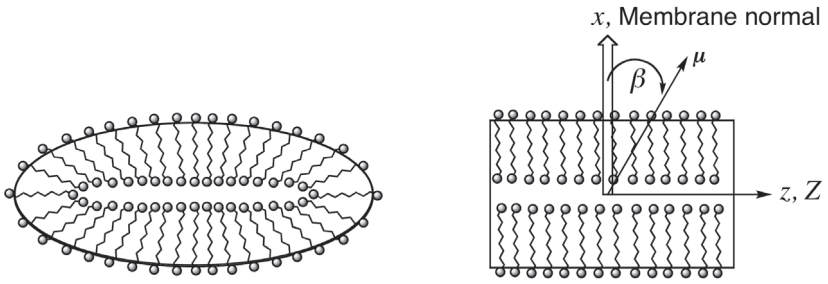

Figure 3.3.3 Left: shear deformed liposome; **Right:** model of deformed liposome. Here, μ is the transition moment of a molecule, x is the membrane normal, z is the long-axis of the cylinder and Z is the macroscopic orientation axis. The orientation of a transition dipole moment μ can be described by the angles β and ψ (not shown - the angle between the projection of μ onto the *y*/*z* plane and *z*). Reproduced by permission of The Royal Society of Chemistry.[21]

By using the local cylinder coordinate system (Figure 3.3.3) the magnitude of the transition moment $\boldsymbol{\mu}$ can be expressed as:

$$\mu = \mu(\cos\beta, \sin\beta\sin\psi, \sin\beta\cos\psi)_{\{x,y,z\}} \tag{3.3.10}$$

By definition, the reduced linear dichroism is described by:

$$LD^r = S\,\frac{A_Z - A_Y}{A_{iso}} = 3S\,\frac{(\mu_Z^2 - \mu_Y^2)}{\mu^2} \tag{3.3.11}$$

In this case $\mu_Z = \mu_z$ and μ_Y can be written as a dot product of $\boldsymbol{\mu}$ and the vector for the Y axis in the $\{x, y, z\}$ coordinate system:

$$\mu_Y = \boldsymbol{\mu}\cdot\boldsymbol{Y} = \mu(\cos\beta\sin\gamma + \sin\beta\sin\psi\cos\gamma) \tag{3.3.12}$$

Thus,

$$LD^r = 3S\,(\sin^2\beta\cos^2\psi - \cos^2\beta\sin^2\gamma - \sin^2\beta\sin^2\psi\cos^2\gamma - 2\cos\beta\sin\gamma\sin\beta\sin\psi\cos\gamma)$$

Because both γ and ψ are taking values from 0 to 2π, the averaging over them results in:

$$LD^r = 3S\frac{2\sin^2\beta - 2\cos^2\beta - \sin^2\beta}{4} = \frac{3}{4}S(1 - 3\cos^2\beta) \tag{3.3.13}$$

For the transition moments inserted into the cylinder, β = 0° giving the minimum value for $LD^r = -\frac{3}{2}S$. While if the transition moments lies on the surface of the cylinder then β = 90° giving the maximum value of $LD^r = \frac{3}{4}S$. In this thesis the above equation was used for experiments with flow-oriented liposomes and bicelles.

Orientation triangle

In a general case of uniaxial orientation of any molecule the following equation holds in the orthogonal coordinate system:

$$LD^r(\lambda) = \frac{LD(\lambda)}{A(\lambda)} = 3\left(\frac{S_{zz}\varepsilon_z(\lambda)+S_{yy}\varepsilon_y(\lambda)+S_{xx}\varepsilon_x(\lambda)}{\varepsilon_z(\lambda)+\varepsilon_y(\lambda)+\varepsilon_x(\lambda)}\right) \quad (3.3.14)$$

where $\varepsilon_z(\lambda)$ etc. are the extinction coefficients at wavelength λ related to light polarized parallel to the respective coordinate axis; and S_{xx} etc. are the order parameters describing the orientation of the respective axis. The order parameters are not independent and $S_{zz}+S_{yy} + S_{xx} = 0$. Also, z is defined to be the molecular axis with highest S_{zz} value, and x to be the one with the lowest value, i.e. $S_{zz} \geq S_{yy} \geq S_{xx}$.

When the orientation behaviour of the solute molecules is of interest sometimes it is practical to display S_{zz} and S_{yy} values plotting them against each other in an orientation triangle (Figure 3.3.4). The sides of this triangle set limits for two different types of orientation: "disc-like" alignment can be found in the vicinity of the side where $S_{zz} = S_{yy}$ and "rod-like" behaviour near the side $S_{yy} = -0.5\, S_{zz}$. Plotted S_{zz} and S_{yy} values for molecules that behave neither as rods or discs may be found anywhere inside the triangle. The orientation behaviour, presented in Figure 3.3.4, results from molecules oriented in stretched polyethylene (PE) matrices. Other polymer or lipid hosts will probably give different alignment behaviour of the oriented solutes.[56]

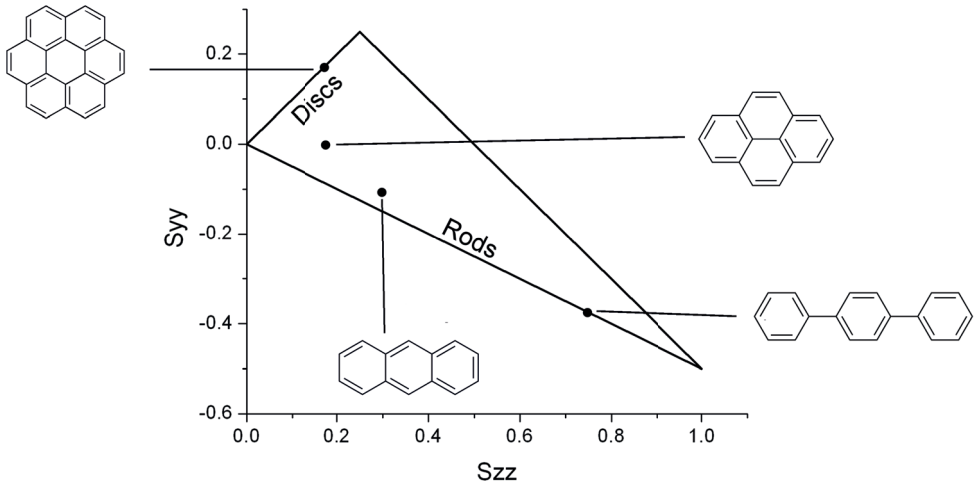

Figure 3.3.4 Orientation triangle for planar or rod-like aromatic molecules oriented in stretched polyethylene films.[57] The molecules are shown with their z-axes horizontal.

3.4 Dynamic Light Scattering

Dynamic light scattering (DLS), also known as Photon Correlation Spectroscopy (PCS), is a technique commonly used to determine the size and structure of colloidal particles. In a typical DLS experiment (Figure 3.4.1) a diluted sample solution is illuminated by a monochromatic, coherent light, I_o, with a wavelength that is not absorbed by the particles in the sample. Most of the light passes trough the sample, except for a small fraction, which strikes the colloidal particles and scatters in different directions. The angular dependence of the I_θ intensities can be described in terms of the scattering vector $|\vec{q}|$:

$$|\vec{q}| = \frac{4\pi n}{\lambda} \sin\frac{\theta}{2} \qquad (3.4.1)$$

where n is the refractive index of the sample, λ - the wavelength of the incident light and θ - the observation angle.

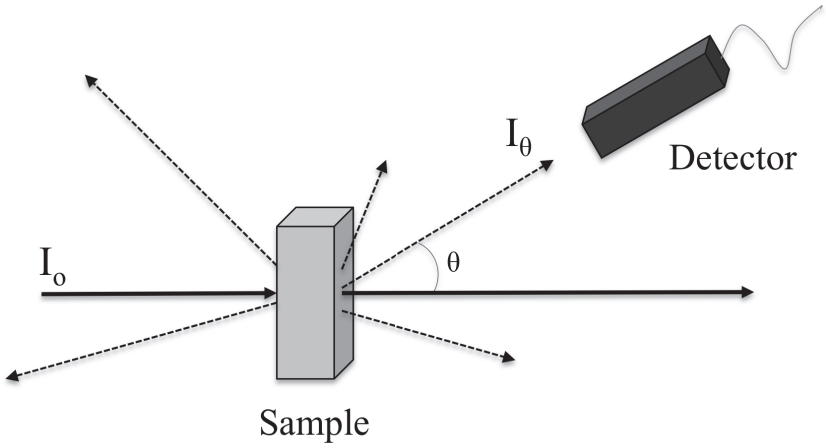

Figure 3.4.1 A schematic representation of the DLS experimental setup

The scattering intensity I_θ of each specific direction varies with time due to the Brownian motion of the particles (Figure 3.4.2). These fluctuations can be monitored by an instrument component called a digital correlator, which measures the degree of similarity between two signals over a period of time. Thus measuring the scattering intensity at a certain angle θ an autocorrelation curve (Figure 3.4.2) can be generated according to:

$$g^2(q,\tau) = \frac{\langle I(t)I(t+\tau)\rangle}{\langle I(t)\rangle^2} \qquad (3.4.2)$$

where $g^2(q, \tau)$ is the autocorrelation function at a particular vector q, $I(t)$ is the scattering intensity at the time t, and τ is delay in time. At short time delays, the positions of the particles are nearly unchanged giving high correlation between $I(t)$

and $I(\tau)$ and therefore $g^2(q, \tau) \approx 1$. When the time delay increases the original positions of the particles change significantly due to the Brownian motion until there is no correlation between the initial and final position giving $g^2(q, \tau) = 0$. Large particles are generally moving slower than small ones thus the decay rate will be much faster for small particles than for large. Therefore the rate of the correlation decay is related to the particle size and for spherical particles it is described by:

$$g^{(2)}(\tau) = A\left[1 + Be^{-2q^2D\tau}\right] \quad (3.4.3)$$

where A and B are correction factors related to the experimental set-up, q is the scattering vector and D the translational diffusion coefficient of the particles in the sample.

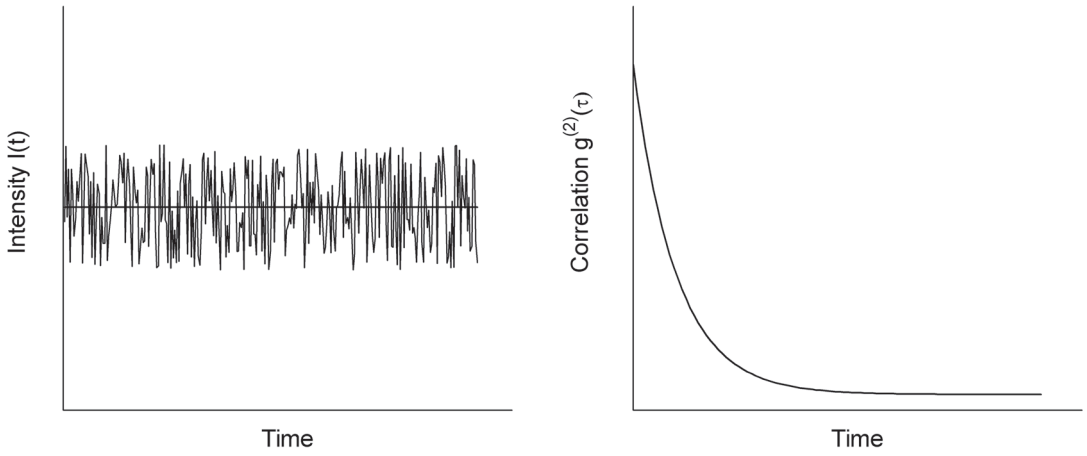

Figure 3.4.2 Principles of DLS. **Left:** The time-dependent intensity variation of the scattered light. **Right:** A typical shape of the correlation function.

For mono-dispersed samples the diffusion coefficient D (Eq. 3.4.3) can be determined by fitting single exponential to the correlation function. The determination of the diffusion coefficient allows estimation of the particle size by using the Stokes-Einstein equation, assuming spherical shape of particles:

$$R_H = \frac{k_B T}{6\pi\eta D} \quad \text{(Equation 3.4.4)}$$

where R_H is the hydrodynamic radius, k_B the Boltzmann's constant, T the absolute temperature and η the viscosity of the sample. In the articles included in this Thesis DLS is mainly used for size determination of liposomes (Papers I-II).

4. ORIGINAL WORK

This section presents a short summary of the papers included in this thesis (Papers I-V). The most important results and conclusions from each paper are summarized and discussed.

4.1 Characterization of flow-oriented liposomes

The flow-oriented 100-nm DOPC liposomes are generally used as a lipid model for linear dichroism measurements. However this membrane model still require further characterization because little is known about what happens to liposomes exposed to shear-deformation. Additionally it is the macroscopic orientation of lipid bilayers that is generally considered in LD while the microscopic orientation of the membrane is usually ignored. This is because, to date, it has not been possible to separate these two parameters using liposomes as a membrane system. Finally the high light scattering and the poor lipid bilayer alignment of liposomes are some of the disadvantages of this system that are in need of improvement. In Papers I and II we present our results from the on-going characterization of DOPC liposomes focusing on such issues as alignment enhancement and investigating the microscopic orientation of lipid bilayers.

4.1.1 Improving the macroscopic alignment

To improve 100-nm DOPC liposomes as membrane models for LD, we tested different concentrations of sucrose, to achieve refractive index matching and a better alignment of the sample. We also tested the behaviour of liposomes at higher shear forces than usually applied (3100 s^{-1}). While working with samples containing sucrose, we could observe a time-dependent increase of the LD signal in some of the measurements indicating an increase of the lipid-phase alignment. This phenomenon was more pronounced for high viscosity samples (i.e. 50% w/w sucrose) and clearly dependent on the applied shear force. The detected time-dependency of the probe-alignment was not previously observed or reported and therefore unexpected for this liposomal system.

In Paper I, we demonstrated a four-fold increase of lipid-phase alignment for high viscosity liposomal solutions resulting from prolonged shear-force application. Also, we presented evidence for shear-induced membrane fusion of liposomes, which is probably the reason behind the increase in liposomal alignment. In this study, apart from LD measurements, dynamic light scattering (DLS) and fluorescence resonance

energy transfer (FRET) were used to characterize shear-flow liposomes. In order to investigate the effect of the solution viscosity on the liposome alignment, five samples with different sucrose concentration (0–50 wt%) were investigated in this study.

Figure 4.1.1A shows a time-dependent growth of the LD signal for a shear-oriented sample containing 50 wt% sucrose and at a shear force of 6200 s^{-1}. The peak LD at 350 nm (Fig. 4.1.1B) displays an almost four-fold increase of the signal over 90 min. Also it can be seen that the major increase takes place during the first 40 min while at 80 min the signal almost reaches a plateau. Figure 4.1.1B presents a series of measurements, which investigates the effect of viscosity on the sample alignment. Samples with 0, 10 and 30 wt% sucrose show no significant changes in the signal over time, while samples with 40 and 50 wt% sucrose display a rapid increase of the LD.

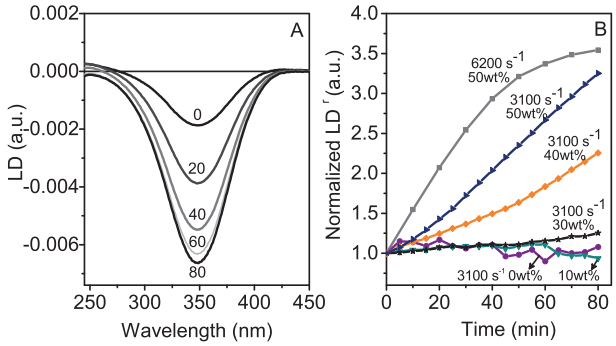

Figure 4.1.1. (A) LD of retinoic acid incorporated in DOPC liposomes in 50 wt% of sucrose under the shear force of 6200 s^{-1} at initial times 0 and after 20, 40, 60 and 80 min. (B) Variation over time of the LD^r values at 350 nm of retinoic acid incorporated in DOPC liposomes in the presence of 0, 10, 30, 40, and 50 wt% of sucrose under an applied shear force of 3100 s^{-1} compared to the sample with 50 wt% sheared at 6200 s^{-1}. Note that LD^r values are positive due to their normalization to the first measured point (considered as the 0 min point) for better comparison.

DLS measurements (Fig. 4.1.2) show that the initial size of the liposomes in 50 wt% buffer changes during 120 min under an applied force of 6 200 s^{-1}. Thus at time 0 the liposomes have an average diameter of 120 nm, and after two hours under shear flow their size increases to approx. 360 nm.

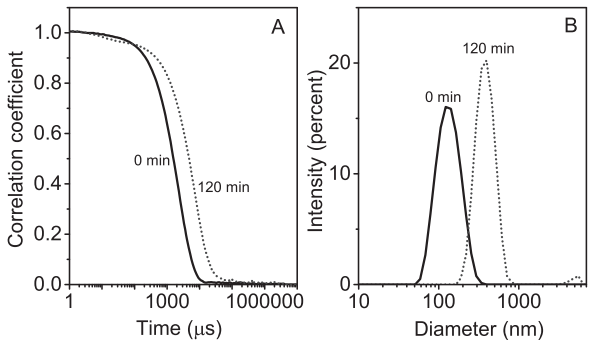

Figure 4.1.2. Effect of shear flow at 6200 s^{-1} on the size of DOPC liposomes prepared in 50 wt% sucrose: (A) dynamic light scattering autocorrelation function and (B) intensity size distribution before and after shearing for 2 h.

The fusion assay, based on FRET between labeled lipids, was performed (see Paper I for details)[54] and shows a rapid mixing of the lipids under shear flow (Figure 4.1.3). The most rapid lipid mixing occurred at 6 200 s^{-1} (Fig. 4.1.3A) resulting in 76% lipid mixing after 20 min and 100% within 1 hr.

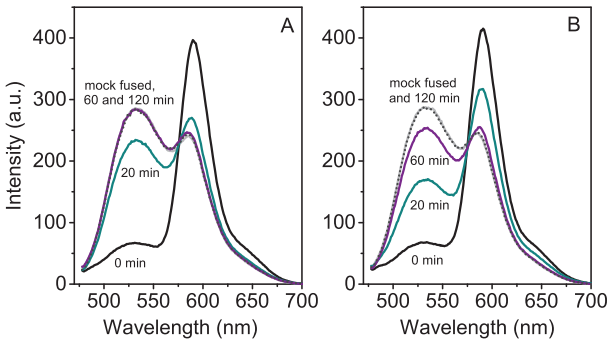

Figure 4.1.3. FRET efficiency, in 50 wt% sucrose buffer, of NBD-PE/Rh-PE labeled liposomes mixed with unlabeled liposomes before (black line) and after rotating-flow at 6200 s^{-1} (A) and 3100 s^{-1} (B), for 20 minutes (dark cyan), 1 hour (purple) and 2 hours (gray dotted line). The spectrum of mock fused liposomes, corresponding to 100% lipid mixing, is shown in light gray (overlapped by the spectra at 1h and 2 h in A and with the spectrum at 2 hours in B).

In summary Paper I describes how mechanical forces can lead to mixing of lipid bilayers. The rapid shear-induced membrane fusion takes place in samples prepared in high viscosity buffers (40–50 wt% sucrose). The membrane fusion leads to four-fold increase in the lipid bilayer orientation and therefore to an increase in the LD signal, resulting in the maximum flow-alignment observed for the liposomal systems.

The main outcome of Paper I, besides high flow-alignment, is the demonstration of lipid-bilayer fusion achieved without any addition of catalysing agents. This is in contrast to previous research showing that addition of certain molecules or ions (poly-(ethylene glycol), dextran, multivalent ions) may be needed in order to induce membrane fusion.[58–61] Instead, in this paper, the membrane fusion was achieved by using high viscosity samples (5.2 and 12.5 cP for 40 and 50 wt% sucrose)[62] in combination with shear rates at or above 3100 s^{-1}. The resulting orientation factor after one hour under the shear force, was $S = 0.25$ which is four times higher than the initial value $S \approx 0.07$. Noticeably the typical orientation factors previously calculated for flow-oriented liposomes are between 0.033 and 1.[6,22]

In conclusion, the described experiments enable, among others, studies on how vesicles behave in viscous media, especially in the presence of fusion proteins and different types of shear forces. This may give novel insights about mechanisms behind this vital biological process.

4.1.2 Investigating the microscopic alignment of model membranes

The macroscopic alignment of liposomes depends on, among other factors, external stress, temperature and lipid composition. These factors also influence the lipid order at the microscopic level. Because characteristics of many membrane-associated biomacromolecules are closely related to changes in the lipid membrane, there is a need for a rapid and convenient characterization of local microscopic changes occurring in a lipid bilayer.

In Paper II, the flow-LD technique was used to track the changes in local lipid ordering in liposomes upon variation of two parameters: cholesterol concentration (0–40%) and applied shear flow (160–3100 s^{-1}). The local ordering was followed by monitoring the change of the ratio between the two orthogonal transition moments of pyrene. Additional probe molecule, curcumin, was used for determination of the macroscopic order of the lipid bilayer. The latter probe was intentionally used to avoid spectral overlap with pyrene.

Figure 4.1.4 summarizes all LD data collected for soybean lipid samples with cholesterol concentrations between 0 – 40% and shear-flow between 80–3100 s^{-1}.

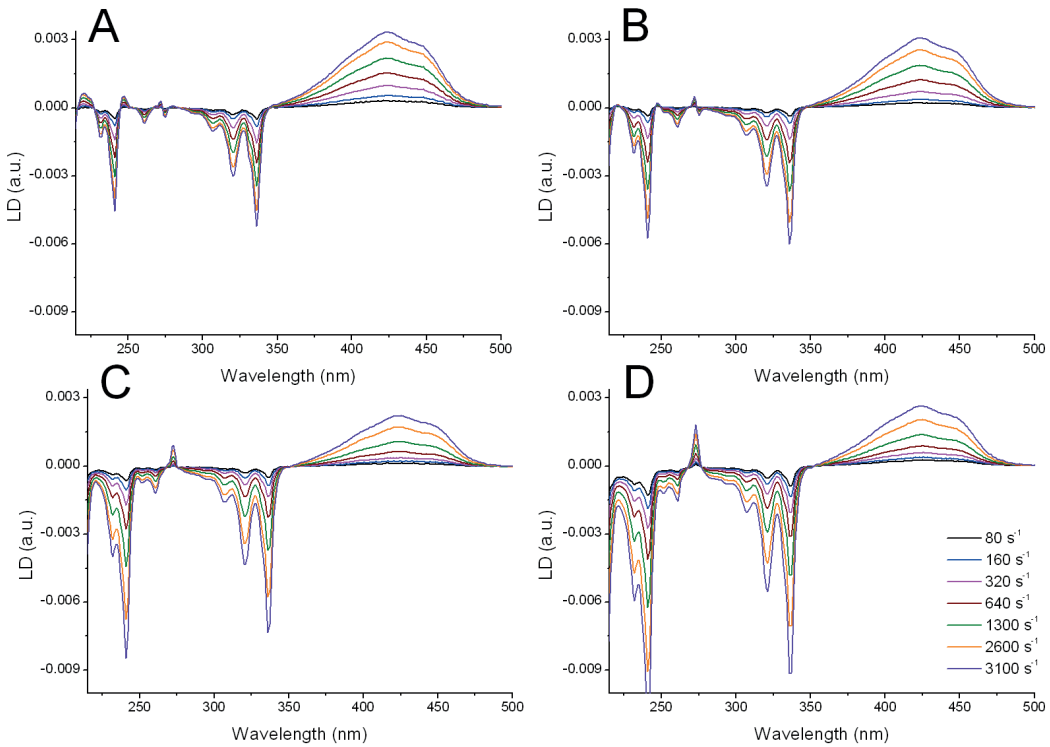

Figure 4.1.4. LD spectra of pyrene (200-350 nm) and curcumin (350-500 nm) added to soybean liposomes with the following cholesterol concentrations: (A) 0%, (B) 10%, (C) 20% and (D) 40%. The alignment shear-force was varied for each sample between 80 and 3100 s^{-1}.

For each of the four investigated samples, increased shear rates are predictably increasing the orientation of the lipid bilayers and consequently the strength of the LD for both pyrene and curcumin. Also samples with higher cholesterol content

demonstrate higher alignment of the pyrene while curcumin orientation does not show such strong and clear dependency on the cholesterol content. Remarkably, the shape of the pyrene peak at 273 nm changes significantly with increasing cholesterol concentration. Figure 4.1.5 shows this trend by presenting the highest LD values of the 273 nm peak for each sample (0%, 10%, 20% and 40%) at 3100 s^{-1}.

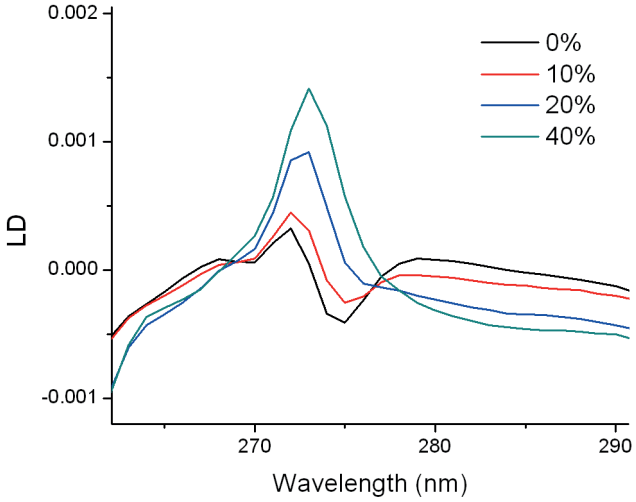

Figure 4.1.5. LD signal of pyrene at 273 nm for samples with cholesterol concentrations from 0 to 40% and at a shear-flow of 3100 s^{-1}.

Further, the change of the peaks from the long-axis transition moments of curcumin (at 424 nm) and pyrene (at 337 nm) show a linear dependency on the shear force (Figure 4.1.6). On the other hand, plotting LD^r of the short-axis transition of pyrene (273 nm) versus LD^r peak values of curcumin (424 nm) reveals nonlinear behavior for some of the samples (Figure 4.1.7).

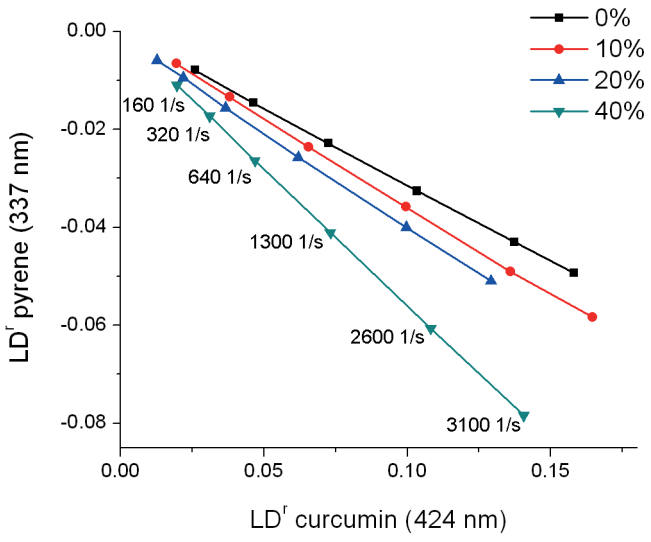

Figure 4.1.6. Peak LD^r values of pyrene at 337 nm plotted versus peak LD^r values of curcumin at 424 nm for samples containing 0%, 10%, 20%, 40% cholesterol and the shear flows between 160–3100 s^{-1}.

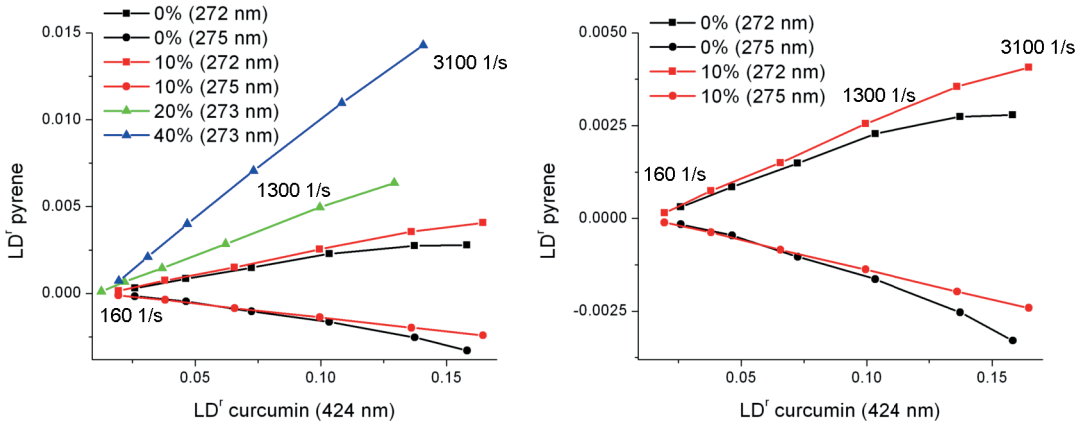

Figure 4.1.7. (Left) Peak LD^r values of pyrene at 272–275 nm plotted versus peak LD^r values of curcumin at 424 nm for samples containing 0%, 10%, 20%, 40% cholesterol and the shear flows between 160–3100 s^{-1}. (Right) Peak values of pyrene and curcumin for samples with 0% and 10% cholesterol plotted as a function of the reduced LD of curcumin at 424 nm.

Figure 4.1.8 represents the orientation triangle with all calculated orientation parameters, S_{yy} and S_{zz}, of the two orthogonal transition moments of pyrene. The measured values are mostly located below the zero axis of the S_{yy} indicating a weak tendency towards rod-like behavior of pyrene alignment for all investigated samples. Noticeably samples with 0% and 10% cholesterol also have positive values of S_{yy} indicating a disk-like character of the short-axis orientation.

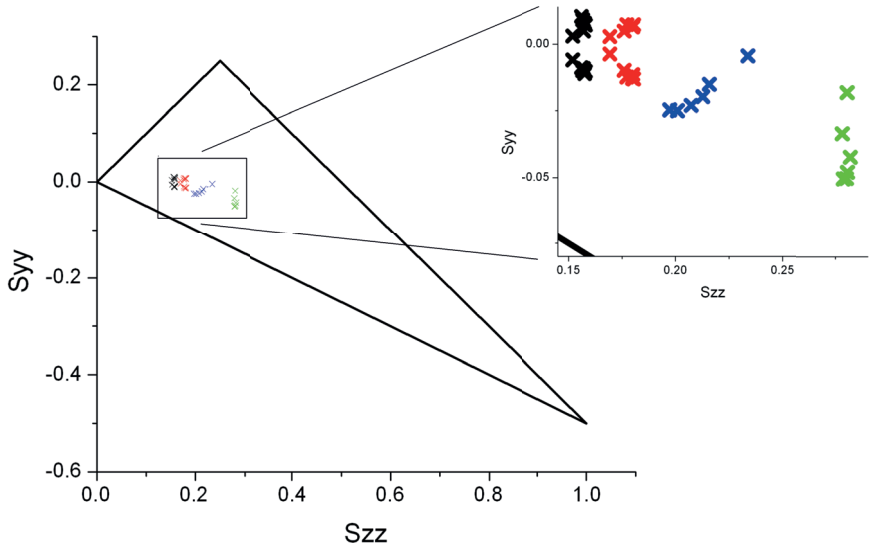

Figure 4.1.8. Orientation triangle containing all measured values of S_{yy} and S_{zz} from two orthogonal transition moments of pyrene for samples oriented by a shear-force 160–3100 s^{-1} and cholesterol concentration of 0% (black), 10% (read), 20% (blue) and 40% (green).

Figure 4.1.9 summarizes the S_{yy} and S_{zz} parameters for different cholesterol concentrations as a function of shear force. It can be noted that negative values of S_{yy} grow both with rising cholesterol concentration and increasing shear force. At the same time S_{zz} values show a clear increase of the orientation at higher cholesterol concentrations while the increase of shear force has a more complex effect on the orientation factors. For 0% and 10% samples the orientation slightly increases with rising shear rate; for samples with 20% cholesterol the orientation decreases; finally S_{zz} factor for samples with 40% cholesterol appears to be unaffected by the rising of shear force and stay more or less constant over the investigated interval 160–3200 s^{-1}.

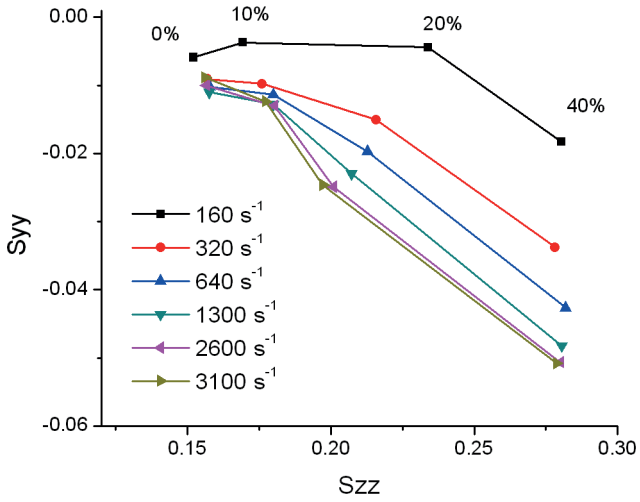

Figure 4.1.9. Orientation triangle containing all measured values of S_{yy} and S_{zz} from two orthogonal transition moments

The split LD peak at 273 nm (Figure 4.1.5) suggests a distribution between slightly different surrounding environments and orientations of the short-axis transition (B_b) of pyrene. Occurrence of two peaks is probably a result of an overlap of a large number of LD spectra with different signs and with slight energy shifts relative to each other. The negative red-shifted LD at 275 nm (Figure 4.1.5) corresponds to the B_b transition being slightly parallel with the lipid chains, resulting in an arrangement with the largest polarizability. The positive LD at 272 nm corresponds to the perpendicular orientation of the B_b transition relative to the lipid chains. In this configuration lipid chains have less interaction with the B_b transition, which results in the blue shift of the LD band.

Overall the experimental data reveal that pyrene can be used for detection of small changes of the lipid order at the molecular level. The changes in the lipid packing by addition of the membrane-stiffening cholesterol can be reflected by the magnitude of the two orthogonal transition moments of pyrene. Likewise it is possible to monitor the effect of external shear stress on the microscopic ordering of the lipid bilayer.

4.2 Bicellar Lipid Mixtures: introducing new membrane model for LD

4.2.1 Proof of concept: flow-alignment of bicelles

During the past decades, the multi-lipid bicellar system, i.e. bicelles, has emerged as promising biological mimetic membrane model used e.g. for structural studies of membrane-associated proteins.[23,63] However most of the applications of this membrane model has been limited to spectroscopic techniques such as NMR and magnetic sample orientation.[23,25,63–65] In Papers III and IV we proposed the use of bicelles for LD measurements. The alignment of the lipid phase was investigated using such membrane probes as retinoic acid (RetA) and pyrene.

In paper III, the flow alignment of bicelles was investigated using a common binary bicellar mixture composed of DHPC and DMPC lipids with a mixing ratio of 3.2. Upon application of the shear force the LD signal of both membrane probes could be successfully recorded confirming the lipid phase alignment (Figure 4.2.1). The LD data collected from the RetA sample displayed a distinct negative LD peak at 354 nm, while the data from the pyrene sample showed a positive peak at 272 nm and a negative peak at 339 nm (Figure 4.2.1 A and B). Based on these observations it could be concluded that the membrane surface normal of the bicellar system was mainly oriented perpendicular to the macroscopic orientation (see Paper III).

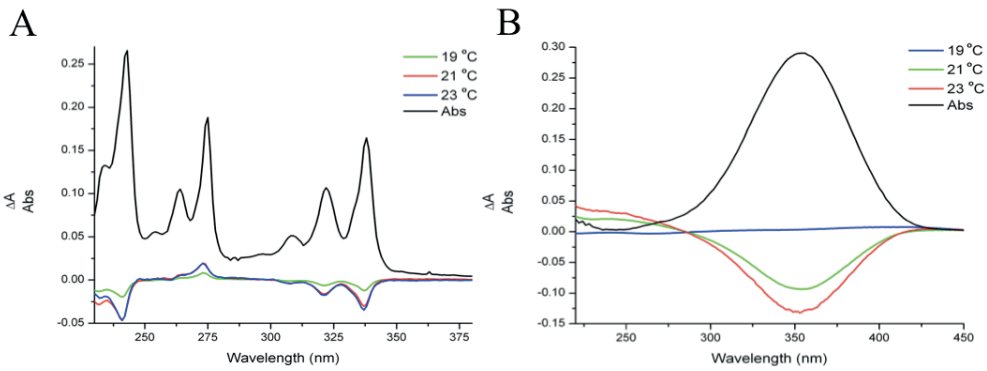

Figure 4.2.1. Absorbance and LD spectra for the bicellar mixtures with: pyrene (A); retinoic acid (B).

Knowing that the morphology of the bicellar mixtures depends on temperature,[64] flow sample alignment was also investigated in a broader temperature range between 15–50 °C. Figure 4.2.2A summarises the temperature dependence of the LD signal, presenting the peak values of the membrane probes. When the temperature was increased from 15 °C, the first LD signals indicating the alignment of the membrane probes were observed at 19 °C. Further increase of the temperature in the interval 19–

23 °C produced a quick rise of the LD signal, which reached its maximum at 23 °C. A subsequent rise of the temperature to 25–50 °C resulted in a rapid decline of the signal. The highest alignment of the RetA was observed at 23 °C, resulting in the macroscopic orientation parameter S = 0.3, which was three to ten times higher than the orientation achieved using DOPC liposomes (S = 0.033–0.1),[6,22] the most commonly used lipid system for flow-LD.

The flow orientation of a membrane-associated protein, cytochrome c, in bicellar mixtures was studied by the LD technique in order to explore possible biological applications of the DMPC/DHPC membrane model. The results presented in Figure 4.2.2B indicate a good alignment of the protein molecules. The LD signal displays a shape that is characteristic for the oxidized form of the cyt *c*, which was previously observed with LD measurements using liposomes.[7] The quality of the observed signal allowed resolving the structural information in the aromatic (200–300 nm) as well as in the heme Soret regions (400nm and 500–600 nm). This is a clear advantage of the bicelle membrane system, because the aromatic band of the protein was hidden by high light scattering in the previous measurements made with liposomes.

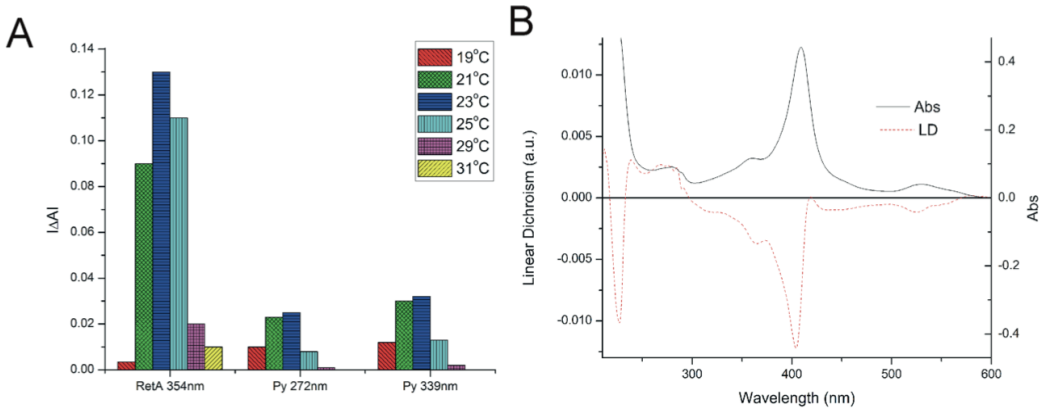

Figure 4.2.2 (A) Absolute peak values of pyrene and retinoic acid at different temperatures and the constant shear gradient of 900 s^{-1}; (B) Absorbance and LD of cytochrome c at 27°C and a shear gradient of 600 s^{-1}.

4.2.2 Optimization of parameters affecting bicelle flow alignment

While working with DMPC/DHPC system in Paper III, we noticed that besides the temperature, parameters such as lipid concentration and applied shear force were among other important factors influencing the flow alignment. Also in Paper III, the analysis was limited to the DMPC/DHPC mixtures with the lipid-mixing ratio of q = 3.2, excluding other common DMPC/DHPC ratios used in the NMR field. Consequently a more extended study was needed in order to determine the influence of those parameters on bicelle orientation. Thus, Paper IV presents a characterization of the bicellar alignment over an extended range of system parameters, such as lipid-mixing ratio, lipid concentration, temperature and applied shear force.

As previously described in Paper III, LD spectroscopy was used to investigate the alignment of the bicellar samples using membrane probes. Samples with three different DMPC/DHPC molar ratios were investigated: q = 2.5, q = 3.2 and q = 4.0. Additionally, four samples were prepared for each ratio with the following lipid concentrations: 3 wt%, 5 wt%, 10 wt% and 20 wt%. By using a Couette cell equipped with speed and temperature control, the behaviour of DMPC/DHPC mixtures was investigated at a broad range of flow gradients and at temperatures between 18–40 °C.

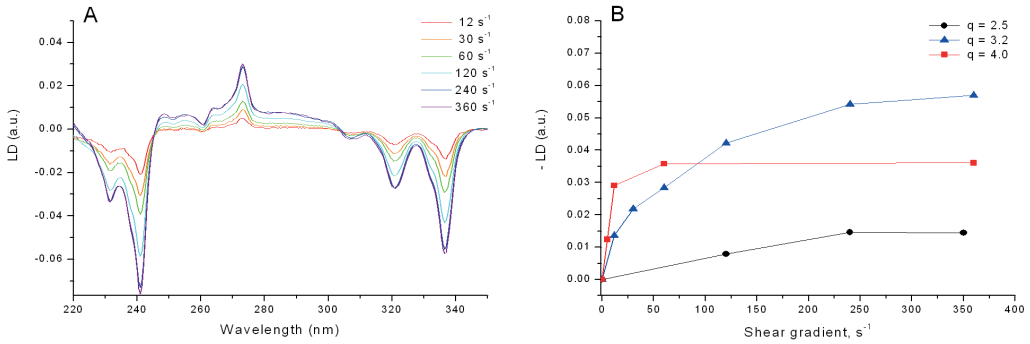

Figure 4.2.3 (A) Change of pyrene LD signal with increase of shear gradient between 12–360 s^{-1}, for the q = 3.2 and l = 5 wt% sample at 25 °C. Color code: 12 s^{-1}: *red*, 30 s^{-1}: *orange*, 60 s^{-1}: *green*, 120 s^{-1}: *cyan*, 240 s^{-1}: *blue*, 360 s^{-1}: *magenta*. (B) Peak values of the LD at 337 nm for q = 2.5 (*black*), q = 3.2 (*blue*) and q = 4.0 (*red*) at varied shear gradient.

LD measurements indicated clearly that a shear gradient variation had a pronounced effect on the alignment of the bicellar samples. Figure 4.2.3A exemplifies the effect of shear gradients on the pyrene orientation added to the q = 3.2 sample at 5 wt% concentration. For this sample, the magnitude of the LD signal grows when the shear gradient increases from 12 to 360 s^{-1}. Likewise the samples with other mixing ratios demonstrate a similar dependency on the shear force. Figure 4.2.3B summarizes the alignment behaviour of all the investigated mixing ratios, by presenting only the

LD peak values at 337 nm arising from one of the pyrene transition moments. While alignment of the q = 2.5 sample demonstrates only a slight increase with shear gradient, both 3.2 and 4.0 samples show rapid and pronounced growth of the LD signal. Also, it can be concluded that the q = 4.0 sample reaches the maximum alignment much quicker than other investigated samples.

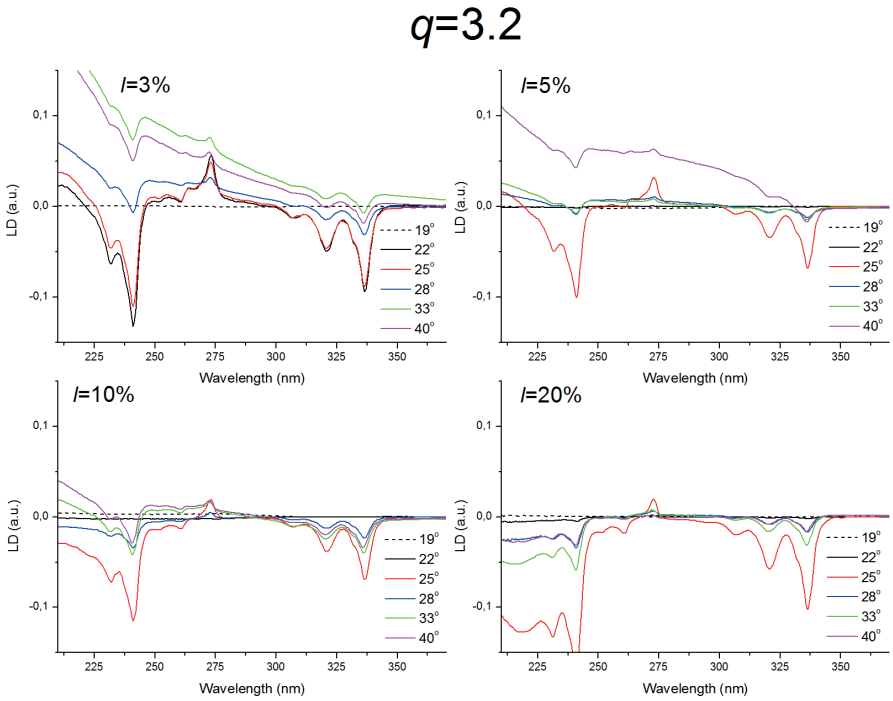

Figure 4.2.4 LD spectra of pyrene probe added to bicellar samples with q = 3.2 and the lipid concentration of 3 wt%, 5 wt%, 10 wt%, 20 wt% at the investigated temperatures. Spectra were recorded at a shear force of 350 s^{-1}; all spectra are normalized to 1 mm pathlength; concentration of pyrene is 50 μM for all samples.

Both the q = 2.5 and 4.0 samples reach a steady-state condition of the alignment in the investigated shear force interval. In contrast, the alignment of the q = 3.2 sample shows a continuing signal growth over the investigated interval. This behaviour is in agreement with our previous results presented in Paper III, which showed a greater orientation of the q = 3.2 samples when higher shear gradients were applied (900 s^{-1}). However increasing shear gradients above 400 s^{-1} resulted in air bubble formation in some of the investigated samples, leading to fluctuating LD signal and high noise-to-signal ratio. Therefore the shear gradient of 350 s^{-1} was estimated to be optimal for most of the samples, giving good alignment and attaining comparability of samples.

The temperature influence on flow alignment was investigated for all bicellar samples used in this study. Figure 4.2.4 shows the LD data illustrating a set of experiments for q = 3.2 samples at various hydrations and temperatures. Similar series of measurements were performed for the samples with the lipid ratios q = 2.5 and 4.0.

Figure 4.2.5 summarizes the experimental results presenting LD^r peak values at 337 nm.

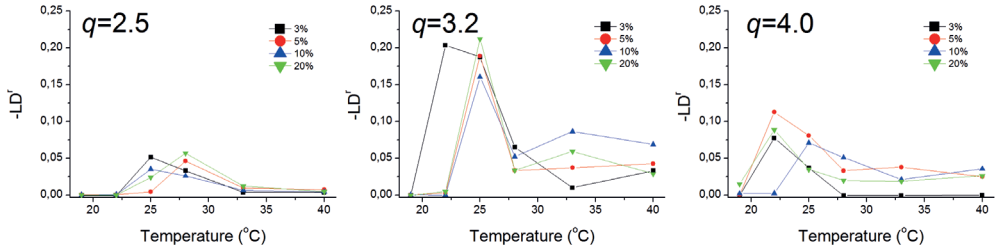

Figure 4.2.5 Temperature dependence of LD^r at 337 nm for pyrene samples with q = 2.5, q = 3.2, and q = 4.0 with lipid concentration between 3–20 wt% and shear force of 350 s^{-1}; all spectra are normalized to 1 mm pathlength; concentration of pyrene 50 μM; l = 3 wt% (*black*), l = 5 wt% (*red*), l = 10 wt% (*blue*), l = 20 wt% (*green*).

Data presented in Figure 4.2.5 reveal some similarities in the alignment behaviour for samples with different lipid molar ratios (q = 2.5, 3.2 and 4.0). All of the samples reach the maximum LD values within the temperature region of 22-28 °C. For all lipid ratios, the LD signals decline at temperatures above 28 °C, and they also show no orientation below 19 °C. It is also noticeable, that the increase in q value from 2.5 to 4.0 leads to lowering the temperature for maximum alignment from ~28 °C to ~22 °C for most of the lipid concentrations. Finally the results in Figure 4.2.5 show that the q = 3.2 samples achieve the highest sample orientation among the other investigated lipid ratios, while the q = 2.5 samples have the lowest alignment. Table 4.1 summarizes the macroscopic orientation parameter S for the investigated samples. The maximum values of S display only minor variations between the samples with the same molar lipid ratio. The maximum value of S = 0.2 is reached by the 3.2 sample, while 2.5 sample shows the lowest orientation with S = 0.7.

The results presented in Papers III and IV demonstrate that DMPC/DHPC bicelles can be efficiently aligned by shear flow. The flow alignment of this membrane model shows a complex behaviour depending on such system parameters as lipid mixing ratio, lipid concentration, temperature and shear gradient. Even though flow-oriented bicelles do not reach as high degree of alignment as bicelles oriented with the magnetic field used in NMR, the ordering of the bicelle phase is still surprisingly high (S = 0.2). In order to achieve the same degree of alignment as presented here, magnetic fields of 4−5 T have to be used.[66]

Table 4.1. The maximum macroscopic orientation parameter (S), and LD^r values calculated for the investigated DMPC/DHPC lipid systems using RetA as a membrane probe.

Molar ratio	Lipid conc. %	$-LD^r$ (at 350 nm)	*S*
q = 2.5	20	0.11	0.07
	10	0.11	0.07
	5	0.14	0.09
	3	0.12	0.08
q = 3.2	20	0.30	0.20
	10	0.28	0.19
	5	0.29	0.19
	3	0.30	0.20
q = 4.0	20	0.20	0.13
	10	0.17	0.11
	5	0.18	0.12
	3	0.15	0.10

When performing spectroscopic measurements involving membrane models, it is important to have a lipid system with low optical contribution to the LD and absorbance spectra. In the case of the most commonly used system, DOPC liposomes this is usually achieved by low lipid concentration (0.1–0.2 wt%) and refractive index matching of buffers by sucrose addition (50 wt%).[5,6,8,22] In Papers III and IV, the DMPC/DHPC samples at much higher lipid concentrations were investigated – 15 to 200 times higher than for liposomal system. While 10 and 20 wt% samples displayed elevated light scattering, the 3–5 wt% samples exhibited low light scattering comparable with that arising from DOPC liposomes. This makes 3–5 wt% samples more suitable for LD and absorbance measurements. Moreover using the same probe concentration with liposomes and bicelles, a lower sample - to - lipid ratio is obtained for the latter, thus minimizing potential probe aggregation and other perturbing effects of probes in the lipid membranes.

A particularly beneficial property of the investigated bicelle system over DOPC liposomes is their considerably higher alignment. The highest achieved bicelle orientation at 350 s^{-1} has an orientation factor of S = 0.2 which is two to six times higher than the orientation factors usually obtained for flow-aligned liposomes (S = 0.033–0.1). [6,22] Moreover, Paper III described even higher orientation with S = 0.3 for DMPC/DHPC q = 3.2 samples aligned by a significantly stronger shear force of 900 s^{-1}. Such strong alignment of bicelles provides significantly higher spectral resolution and therefore can potentially offer more detailed structural information on membrane-associated molecules.

In conclusion in Papers III and IV we demonstrated that bicelles could be efficiently aligned by shear flow. Also the sample composition and systems parameters most suitable for the optical spectroscopy were determined. The bicelles

showed a high degree of orientation providing detailed structural information of small solute molecules. The morphological change of the lipid assemblage was proposed as a possible explanation for the alignment dependency on temperature, lipid concentration and molar ratio. Moreover it was concluded that the temperature region of the highest sample alignment coincided with one of the phase transitions regions characterized by the highest sample viscosity.

The biological application of bicelle was demonstrated in Paper III using LD measurements in samples containing a protein (cytochrome c). Measurements using bicelles as a membrane host allowed resolution of the structural information in the aromatic region (200–300 nm) of the spectrum. The region that was inaccessible when using liposomes as membrane model due to the high light scattering of the sample. Thus flow orientation combined with optical techniques opens up opportunities for future structural and dynamic studies of membrane proteins and other membrane-associated molecules.

4.3 Modelling and probing DNA rare base-pair opening

In living cells, individual DNA base pairs are constantly undergoing a process of disruption and reformation.[33,67] This process is called "DNA breathing" and it mainly occurs due to the weak character of the hydrogen bonds formed between the individual bases.[68–70] Structures, which are adopted during these transient structural fluctuations, include the single- to double-strand junctions, which are believed to be important for the recognition of and binding to regulatory enzymes. Especially those binding motifs are important for control of such essential cellular processes as transcription, replication and recombination.[30]

Generally transient openings of a DNA duplex can be comparable to some of the static imperfectly paired structures. These can include regional un-pairing, loops and junctions, which can be introduced into long DNA by heat denaturation – a process when thermal melting of DNA is followed by rapid cooling. Also the imperfectly paired structures can be introduced into the short DNA fragments by synthesis.

In Paper V we probed transition-state base-pair openings by using static imperfectly paired structures of heat denatured DNA. We used LD spectroscopy and luminescence experiments to compare the threading intercalation of the binuclear ruthenium complex ΔΔ-P (Figure 4.3.1A) into the heat denatured (hd) and the native calf thymus (ct) DNA.

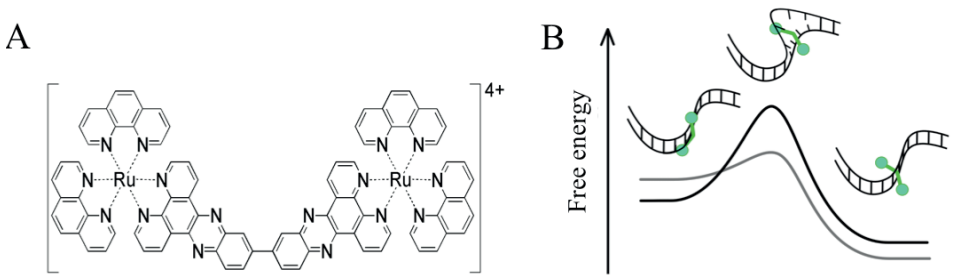

Figure 4.3.1. (A) The chemical structure of the bidppz-bridged binuclear ruthenium complex; (B) Energy diagram illustrating the energetics of the threading rearrangement: groove bound ruthenium complex (left cartoon) that, through a high-energy transition state involving formation of a loop-hole in the duplex, becomes intercalated (right). Threading into hd-DNA (grey) appears to have a lower energy barrier than native ct-DNA (black).

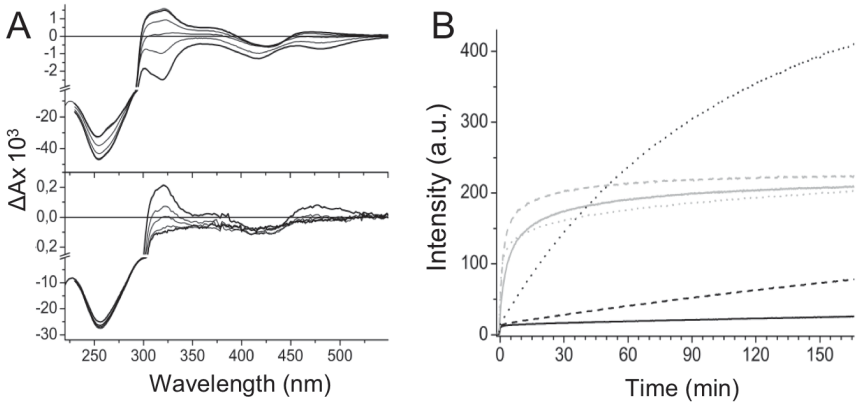

Figure 4.3.2. (A) (Top panel) LD after mixing ΔΔ-P and native ct-DNA; spectrum top to bottom: (at RT) 5 min, 1 h, (at 50 °C) 30 min, 1 h, 4 h, 12 h; (bottom panel) LD after mixing ΔΔ-P and hd-DNA; spectrum top to bottom: (at RT) 1 min, 5 min, 1 h, (at 50 °C) 30 min, 12h). (B) Kinetics after mixing ΔΔ-P and native (black) or hd (grey) ct-DNA at 25 (solid), 37 (dashed) and 50 ºC (dotted).

LD data presented in Figure 4.3.2A shows rapid intercalation of ΔΔ-P into hd-DNA already at room temperature in contrast with the data observed for native ct-DNA. The time-dependent declining of the LD signal caused by ΔΔ-P threading into hd-DNA shows that the complexes are preferentially bound to the less ordered regions of the DNA, such as hairpin loops, mismatched regions etc. In order to follow ΔΔ-P threading into hd-DNA kinetic studies were performed. Results summarized in Figure 4.3.2B illustrate low temperature-dependence of hd-DNA intercalation, which indicate a decrease in activation energy for ΔΔ-P threading (Figure 4.3.1B).

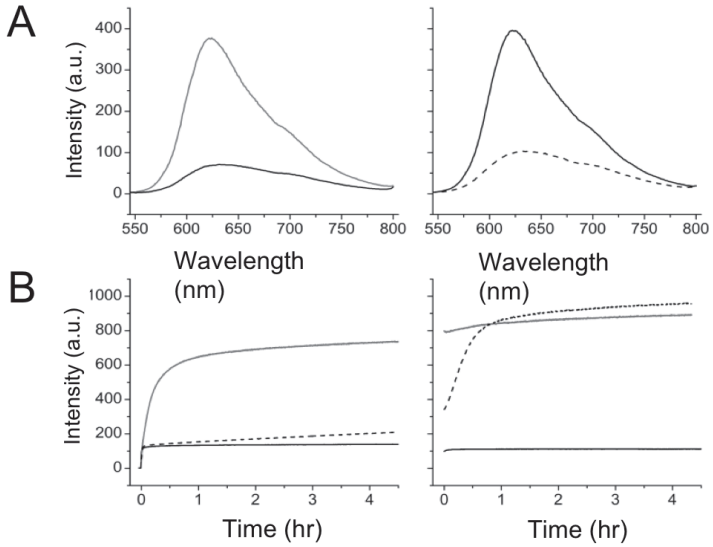

Figure 4.3.3. (A) (To the left) Emission spectrum of ΔΔ-P equilibrated with X = 7 oligonucleotide (black) or poly(dAdT)$_2$ (grey); (to the right) emission spectrum of ΔΔ-P added to a mixture of X = 7 oligonucleotide and poly(dAdT)$_2$ after incubation for 5 h at 25 °C (dashed) and after further heating for 5 h at 50 °C (solid). (B) The evolution of the luminescence increase after mixing at 25 °C (to the left) and upon increase of temperature to 50 °C (to the right) for samples containing ΔΔ-P and X = 7 oligonucleotide (black, solid) or poly(dAdT)$_2$ (grey) only and for sample containing ΔΔ-P and a mixture of the two DNAs (black, dashed).

Due to the fact that less stable AT-rich DNA regions are especially liable for structural changes under the heat denaturation and cooling cycle, a comparison study using a short alternating AT-polymer poly(dAdT)$_2$ was performed. The competition experiment with X = 7 oligonucleotide has shown (Figure 4.3.3) that unpaired structures offer a more attractive site for threading intercalation than paired AT bases. However paired AT regions offer thermodynamically the most favourable intercalation sites. Also we examined how efficiently a small amount of these oligonucleotides can be targeted through threading intercalation in the presence of paired ct-DNA. LD in combination with emission fluorescence has shown a fast rearrangement to intercalation of ΔΔ-P interacting with the loop-containing oligonucleotides (Figure 4.3.4), which indicates a preference for these forms of DNA compared to ct-DNA.

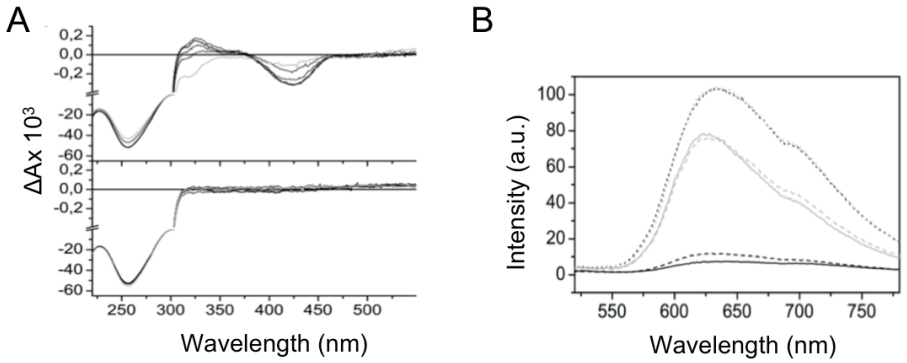

Figure 4.3.4. (A) (Top panel) LD after addition of ΔΔ-P to native ct-DNA only (bottom panel) and with addition of X = 7 oligonucleotide. Spectrum: (at RT) 5 min, 20 min; (at 50 °C) 1 h, 4 h, 12 h (grey). (B) Emission spectrum of samples containing ΔΔ-P and ct-DNA only (solid) or the mixture of ct-DNA and X = 0 (dashed) or X = 7 (dotted) oligonucleotide 20 min after mixing at RT (black) and after heating at 50 °C for 4 h (grey).

In conclusion, the intercalation of a dumb-bell shaped ruthenium complex between two DNA strands is associated to rare, transient duplex openings. Thus binuclear ruthenium complexes can be used to probe local un-pairing of DNA strands. In this paper, we have investigated DNA constructs structurally imitating hypothetical transition states of DNA, in which threading, and unthreading, are shown to be greatly facilitated. The first of the investigated DNA constructs involved improper re-annealed heat-denatured DNA duplex. While intercalation of the ΔΔ-P into native DNA requires hours at elevated temperature, the threading into the improperly re-annealed hd-DNA occurs much faster. This indicates a strong reduction of the activation barriers to intercalation for the imperfectly paired regions, which act as stationary threading portals. The second investigated model for transition states included protruding loops in oligonucleotide duplexes. Experimental results indicate noticeably lowering of the energy barrier for intercalation, resulting in kinetically controlled threading of ΔΔ-P into unpaired sequences. The overall outcome of this paper may have relevance for new strategies for targeting imperfectly matched DNA. Also it may have importance for understanding how DNA "breathing" effects transcription, replication and recombination processes.

5. CONCLUDING REMARKS

The work presented in this thesis aims to develop model systems, which in combination with polarized light spectroscopic methods can be used to study processes occurring in the living cells. Here we present new research concerning certain model systems appropriate for LD studies of both membrane-associated molecules and DNA. We introduce to the LD field, and characterize using LD, a new membrane model, so called bicelles, demonstrating great advantages over other flow-LD membrane systems including small light scattering and good alignment. We investigate how this system behaves depending on temperature, lipid concentration and lipid-mixing ratio. Furthermore, we also examine and exploit an already established model system, liposomes, and report new interesting observations regarding the effect of viscosity and shear flow on liposomal alignment. We show that under a prolonged applied shear-stress the liposomes demonstrate a time-dependent increase of alignment resulting in up to fourfold rise of the LD signal compared with the initial value. Also, we demonstrate, for the first time, that information about the microscopic alignment of the molecules in the flow-aligned bilayers of liposomes can be obtained from flow-LD spectra if certain small organic probe molecules are used, one which reports on the macroscopic order of the membrane and one which probes sensitively its interaction with surrounding molecules in the membrane. Finally, we demonstrate how a simplified DNA model with static unpaired regions can be used for studies of temporary transition-state arrangement of DNA.

The findings presented in this thesis contribute to the basic understanding of the existing model systems but also introduce promising new models, which hopefully will be useful in future LD studies. The improvement of flow alignment of the lipid systems (Papers I, III, IV) opens up for new possibilities for binding geometry studies of the membrane-associated molecules. The method for evaluation of the microscopic orientation (Paper II) may be useful for detecting the effect of the lipid order on the function and changes in membrane proteins. The presented investigation of the transition-state model of DNA (Paper V) may have a relevance to the new emerging strategies for targeting imperfectly matched DNA.

6. ACKNOWLEDGEMENTS

I would like to thank the following people who directly or indirectly contributed to my work:

My supervisor Bengt Nordén for giving me the opportunity to work in his group; for the interesting projects; for good ideas, for support and for giving me freedom to form my work. My co-supervisors Tamás Beke-Somfai, Per Lincoln, and other people who guided and supported me in my work - Sandra Rocha, Pär Nordell and John Tumpane. Thank you, friends and colleagues for creating enjoyable atmosphere and giving me great memories: Anke Dierckx, Magnus Bälter, Bobo Feng, Melina Gilbert, Louise Fornander, Martin Hammarson, Catherine Kitts, Valeria Saavedra, and Jacob Woller. My roommates Jelena and David for creating good working environment. Tore Eriksson for making handy and smart LD-cells. Special thanks to Sandra Rocha, John Tumpane and Tamás Beke-Somfai for proofreading and commenting this thesis. My friends and family for all support.

7. REFERENCES

1. Reymer, A., Frykholm, K., Morimatsu, K., Takahashi, M. & Norden, B. Structure of human Rad51 protein filament from molecular modeling and site-specific linear dichroism spectroscopy. *Proc. Natl. Acad. Sci. U. S. A.* **106,** 13248–13253 (2009).

2. Frykholm, K., Morimatsu, K. & Norden, B. Conserved conformation of RecA protein after executing the DNA strand-exchange reaction. A site-specific linear dichroism structure study. *Biochemistry* **45,** 11172–11178 (2006).

3. Esbjorner, E. K., Oglecka, K., Lincoln, P., Graslund, A. & Norden, B. Membrane binding of pH-sensitive influenza fusion peptides. Positioning, configuration, and induced leakage in a lipid vesicle model. *Biochemistry* **46,** 13490–13504 (2007).

4. Ardhammar, M., Lincoln, P. & Norden, B. Invisible liposomes: Refractive index matching with sucrose enables flow dichroism assessment of peptide orientation in lipid vesicle membrane. *Proc. Natl. Acad. Sci. U. S. A.* **99,** 15313–15317 (2002).

5. Caesar, C. E. B., Esbjorner, E. K., Lincoln, P. & Norden, B. Membrane interactions of cell-penetrating peptides probed by tryptophan fluorescence and dichroism techniques: Correlations of structure to cellular uptake. *Biochemistry* **45,** 7682–7692 (2006).

6. Svensson, F. R., Lincoln, P., Nordén, B. & Esbjörner, E. K. Tryptophan orientations in membrane-bound gramicidin and melittin-a comparative linear dichroism study on transmembrane and surface-bound peptides. *Biochim. Biophys. Acta* **1808,** 219–28 (2011).

7. Caesar, C. E. B., Esbjorner, E. K., Lincoln, P. & Norden, B. Assigning Membrane Binding Geometry of Cytochrome c by Polarized Light Spectroscopy. *Biophys. J.* **96,** 3399–3411 (2009).

8. Esbjorner, E. K., Caesar, C. E. B., Albinsson, B., Lincoln, P. & Norden, B. Tryptophan orientation in model lipid membranes. *Biochem. Biophys. Res. Commun.* **361,** 645–650 (2007).

9. Damianoglou, A. *et al.* The Synergistic Action of Melittin and Phospholipase A2 with Lipid Membranes: Development of Linear Dichroism for Membrane-Insertion Kinetics. *Protein Pept. Lett.* **17,** 1351–1362 (2010).

10. Hicks, M. R., Damianoglou, A., Rodger, A. & Dafforn, T. R. Folding and Membrane Insertion of the Pore-Forming Peptide Gramicidin Occur as a Concerted Process. *J. Mol. Biol.* **383,** 358–366 (2008).

11. Kitts, C. C., Beke-Somfai, T. & Norden, B. Michler's Hydrol Blue: A Sensitive Probe for Amyloid Fibril Detection. *Biochemistry* **50,** 3451–3461 (2011).

12. Morris, K. L. *et al.* Exploring the sequence-structure relationship for amyloid peptides. *Biochem. J.* **450,** 275–283 (2013).

13. Wilhelmsson, L. M., Westerlund, F., Lincoln, P. & Norden, B. DNA-binding of semirigid binuclear ruthenium complex Delta,Delta-{[}mu-(11,11 `-bidppz)(phen)(4)Ru-2](4+): Extremely slow intercalation kinetics. *J. Am. Chem. Soc.* **124,** 12092–12093 (2002).

14. Norden, B., Lincoln, P., Nordell, P., Westerlund, F. & Wilhelmsson, M. DNA-threading intercalation rate studies: Dynamics is an efficient mechanism for biomolecular structure recognition. *J. Biomol. Struct. Dyn.* **24,** (2007).

15. Hooke, R. Micrographia. *Edinburgh Alembic Club (originally Publ. 1665)* (1894).

16. Madigan, M. T. Brock Biology of Microorganisms, 11th edn. (2005).

17. Alberts, B. Molecular Biology of the Cell 4th. (2002).

18. Luckey, M. *Membrane structural biology: with biochemical and biophysical foundations*. (Cambridge University Press, 2008).

19. Lodish, H. *et al.* Membrane Proteins. (2000). at <http://www.ncbi.nlm.nih.gov/books/NBK21570/>

20. Blanco.biomol.uci.edu. Membrane Proteins of Known Structure. (2014). at <http://blanco.biomol.uci.edu/mpstruc/>

21. Bengt Nordén, Alison Rodger, T. D. *Linear Dichroism and Circular Dichroism*. (The Royal Society of Chemistry, 2010).

22. Svensson, F. R., Lincoln, P., Norden, B. & Esbjorner, E. K. Retinoid chromophores as probes of membrane lipid order. *J. Phys. Chem. B* **111,** 10839–10848 (2007).

23. Sanders, C. R. & Landis, G. C. Reconstitution Of Membrane-Proteins Into Lipid-Rich Bilayered Mixed Micelles For Nmr-Studies. *Biochemistry* **34,** 4030–4040 (1995).

24. Beaugrand, M. *et al.* Lipid Concentration and Molar Ratio Boundaries for the Use of Isotropic Bicelles. *Langmuir* **30,** 6162–6170 (2014).

25. Prosser, R. S., Evanics, F., Kitevski, J. L. & Al-Abdul-Wahid, M. S. Current applications of bicelles in NMR studies of membrane-associated amphiphiles and proteins. *Biochemistry* **45,** 8453–8465 (2006).

26. Van Dam, L., Karlsson, G. & Edwards, K. Direct observation and characterization of DMPC/DHPC aggregates under conditions relevant for biological solution NMR. *Biochim. Biophys. Acta-Biomembranes* **1664,** 241–256 (2004).

27. Crick, F. Central Dogma Of Molecular Biology. *Nature* **227,** 561–& (1970).

28. Watson, J. D. & Crick, F. H. C. Molecular Structure Of Nucleic Acids - A Structure For Deoxyribose Nucleic Acid. *Nature* **171,** 737–738 (1953).

29. Blackburn, G. Nucleic acids in chemistry and biology. (2006).

30. Jose, D., Datta, K., Johnson, N. P. & von Hippel, P. H. Spectroscopic studies of position-specific DNA "breathing'' fluctuations at replication forks and primer-template junctions. *Proc. Natl. Acad. Sci. U. S. A.* **106,** 4231–4236 (2009).

31. Peyrard, M. Nonlinear dynamics and statistical physics of DNA. *Nonlinearity* **17,** R1–R40 (2004).

32. Von Hippel, P. H., Johnson, N. P. & Marcus, A. H. Fifty Years of DNA Breathing: Reflections on Old and New Approaches. *Biopolymers* **99,** 923–954 (2013).

33. Altan-Bonnet, G., Libchaber, A. & Krichevsky, O. Bubble dynamics in double-stranded DNA. *Phys. Rev. Lett.* **90,** (2003).

34. Bonnet, G., Krichevsky, O. & Libchaber, A. Kinetics of conformational fluctuations in DNA hairpin-loops. *Proc. Natl. Acad. Sci. U. S. A.* **95,** 8602–8606 (1998).

35. Biver, T. Use of UV-Vis Spectrometry to Gain Information on the Mode of Binding of Small Molecules to DNAs and RNAs. *Appl. Spectrosc. Rev.* **47,** 272–325 (2012).

36. Rajendra, J. *et al.* Quantitation of protein orientation in flow-oriented unilamellar liposomes by linear dichroism. *Chem. Phys.* **326,** 210–220 (2006).

37. Wolfe, A., Shimer, G. H. & Meehan, T. Polycyclic Aromatic-Hydrocarbons Physically Intercalate Into Duplex Regions Of Denatured Dna. *Biochemistry* **26,** 6392–6396 (1987).

38. Sartorius, J. & Schneider, H. J. Supramolecular chemistry .71. Intercalation mechanisms with ds-DNA: binding modes and energy contributions with benzene, naphthalene, quinoline and indole derivatives including some antimalarials. *J. Chem. Soc. Trans. 2* 2319–2327 (1997).

39. Aggarwal, B. B., Sundaram, C., Malani, N. & Ichikawa, H. in *Mol. Targets Ther. Uses Curcumin Heal. Dis.* **595,** (SPRINGER, 2007).

40. Aggarwal, B. B. & Sung, B. Pharmacological basis for the role of curcumin in chronic diseases: an age-old spice with modern targets. *Trends Pharmacol. Sci.* **30,** 85–94 (2009).

41. Patra, D., El Khoury, E., Ahmadieh, D., Darwish, S. & Tafech, R. M. Effect of Curcumin on Liposome: Curcumin as a Molecular Probe for Monitoring Interaction of Ionic Liquids with 1,2-Dipalmitoyl-sn-Glycero-3-Phosphocholine Liposome. *Photochem. Photobiol.* **88,** 317–327 (2012).

42. Payton, F., Sandusky, P. & Alworth, W. L. NMR study of the solution structure of curcumin. *J. Nat. Prod.* **70,** 143–146 (2007).

43. Barton, J. K., Danishefsky, A. T. & Goldberg, J. M. Tris(Phenanthroline)Ruthenium(II) - Stereoselectivity In Binding To Dna. *J. Am. Chem. Soc.* **106,** 2172–2176 (1984).

44. Kumar, C. V, Barton, J. K. & Turro, N. J. Photophysics Of Ruthenium Complexes Bound To Double Helical Dna. *J. Am. Chem. Soc.* **107,** 5518–5523 (1985).

45. Zhang, S., Ding, Y. & Wei, H. Ruthenium Polypyridine Complexes Combined with Oligonucleotides for Bioanalysis: A Review. *Molecules* **19,** 11933–11987 (2014).

46. Muller, W. & Crothers, D. M. Studies Of Binding Of Actinomycin And Related Compounds To Dna. *J. Mol. Biol.* **35,** 251–& (1968).

47. Friedman, A. E., Chambron, J. C., Sauvage, J. P., Turro, N. J. & Barton, J. K. Molecular Light Switch For Dna - Ru(Bpy)2(Dppz)2+. *J. Am. Chem. Soc.* **112,** 4960–4962 (1990).

48. Jenkins, Y., Friedman, A. E., Turro, N. J. & Barton, J. K. Characterization Of Dipyridophenazine Complexes Of Ruthenium(Ii) - The Light Switch Effect As A Function Of Nucleic-Acid Sequence And Conformation. *Biochemistry* **31,** 10809–10816 (1992).

49. Lincoln, P. & Norden, B. Binuclear ruthenium(II) phenanthroline compounds with extreme binding affinity for DNA. *Chem. Commun.* 2145–2146 (1996).

50. Onfelt, B., Lincoln, P. & Norden, B. Enantioselective DNA threading dynamics by phenazine-linked {[}Ru(phen)(2)dppz](2+) dimers. *J. Am. Chem. Soc.* **123,** 3630–3637 (2001).

51. Hollas, J. M. *Modern Spectroscopy*. (Wiley, 2013).

52. Lakowicz, J. R. *Principles of fluorescence spectroscopy*. *Princ. Fluoresc. Spectrosc.* 1–954 (Springer, 2006).

53. Berne, B. J. & Pecora, R. *Dynamic light scattering: with applications to chemistry, biology, and physics*. (Dover Publications, 2000).

54. Düzgüneş, N., Faneca, H. & de Lima, M. P. in *Liposomes SE - 16* (ed. Weissig, V.) **606,** 209–232 (Humana Press, 2010).

55. Rodger, A. *Circular dichroism and linear dichroism /*. (Oxford University Press,, 1997).

56. Davidsso.A & Norden, B. New Details In Polarized Spectrum Of Naphthalene By Means Of Linear Dichroism Studies In Oriented Polymer Matrices. *Chem. Phys. Lett.* **28,** 221–224 (1974).

57. Norden, B. Applications of Linear Dichroism Spectroscopy. *Appl. Spectrosc. Rev.* **14,** 157–248 (1978).

58. Macdonald, R. I. Membrane-Fusion Due To Dehydration By Polyethylene-Glycol, Dextran, Or Sucrose. *Biochemistry* **24,** 4058–4066 (1985).

59. Hui, S. W., Kuhl, T. L., Guo, Y. Q. & Israelachvili, J. Use of poly(ethylene glycol) to control cell aggregation and fusion. *Colloids And Surfaces B-Biointerfaces* **14,** 213–222 (1999).

60. Arnold, K., Ohki, S. & Krumbiegel, M. Interaction Of Dextran Sulfate With Phospholipid Surfaces And Liposome Aggregation And Fusion. *Chem. Phys. Lipids* **55,** 301–307 (1990).

61. Wilschut, J. & Hoekstra, D. Membrane-Fusion - From Liposomes To Biological-Membranes. *Trends Biochem. Sci.* **9,** 479–483 (1984).

62. Asadi, M. *Beet-Sugar Handbook*. (Wilay-Interscience, 2007).

63. Gabriel, N. E. & Roberts, M. F. Spontaneous Formation Of Stable Unilamellar Vesicles. *Biochemistry* **23,** 4011–4015 (1984).

64. Katsaras, J., Harroun, T. A., Pencer, J. & Nieh, M. P. "Bicellar" lipid mixtures as used in biochemical and biophysical studies. *Naturwissenschaften* **92,** 355–366 (2005).

65. Nieh, M. P. *et al.* Magnetically alignable phase of phospholipid Bicelle mixtures is a chiral nematic made up of wormlike micelles. *Langmuir* **20,** 7893–7897 (2004).

66. Liebi, M. *et al.* Alignment of Bicelles Studied with High-Field Magnetic Birefringence and Small-Angle Neutron Scattering Measurements. *Langmuir* **29,** 3467–3473 (2013).

67. Frankkamenetskii, M. Dna-Structure - Physicists Retreat Again. *Nature* **328,** 108 (1987).

68. Yakovchuk, P., Protozanova, E. & Frank-Kamenetskii, M. D. Base-stacking and base-pairing contributions into thermal stability of the DNA double helix. *Nucleic Acids Res.* **34,** 564–574 (2006).

69. Krueger, A., Protozanova, E. & Frank-Kamenetskii, M. D. Sequence-dependent basepair opening in DNA double helix. *Biophys. J.* **90,** 3091–3099 (2006).

70. Every, A. E. & Russu, I. M. Probing the role of hydrogen bonds in the stability of base pairs in double-helical DNA. *Biopolymers* **87,** 165–173 (2007).